THE ANALYSIS OF LOW-PROFILE, BROADBAND, MONOPOLE, VEHICLE ANTENNAS AND MATCHING NETWORK SYNTHESIS

BY

STEVEN DONALD EIKEN

B.S., United States Air Force Academy, 1990

THESIS

Submitted in partial fulfillment of the requirements
for the degree of Master of Science in Electrical Engineering
in the Graduate College of the
University of Illinois at Urbana-Champaign, 1993

Urbana, Illinois

REPORT DOCUMENTATION PAGE

Form Approved
OMB No 0704-0188

1. AGENCY USE ONLY (Leave blank)	2. REPORT DATE	3. REPORT TYPE AND DATES COVERED
	1993	THESIS/DISSERTATION

4. TITLE AND SUBTITLE
The Analysis of Low-Profile, Broadband, Monopole, Vehicle Antennas and Matching Network Synthesis

5. FUNDING NUMBERS

6. AUTHOR(S)
Steven Donald Eiken

7. PERFORMING ORGANIZATION NAME(S) AND ADDRESS(ES)
AFIT Student Attending: Univ of Illinois at Urbana-Champaign

8. PERFORMING ORGANIZATION REPORT NUMBER
AFIT/CI/CIA- 93-051

9. SPONSORING/MONITORING AGENCY NAME(S) AND ADDRESS(ES)
DEPARTMENT OF THE AIR FORCE
AFIT/CI
2950 P STREET
WRIGHT-PATTERSON AFB OH 45433-7765

10. SPONSORING/MONITORING AGENCY REPORT NUMBER

11. SUPPLEMENTARY NOTES

12a. DISTRIBUTION/AVAILABILITY STATEMENT
Approved for Public Release IAW 190-1
Distribution Unlimited
MICHAEL M. BRICKER, SMSgt, USAF
Chief Administration

12b. DISTRIBUTION CODE

13. ABSTRACT (Maximum 200 words)

14. SUBJECT TERMS	15. NUMBER OF PAGES	16. PRICE CODE
	79	

17. SECURITY CLASSIFICATION OF REPORT	18. SECURITY CLASSIFICATION OF THIS PAGE	19. SECURITY CLASSIFICATION OF ABSTRACT	20. LIMITATION OF ABSTRACT

ABSTRACT

The characteristics of low-profile, broadband, monopole vehicle antenna designs are obtained and evaluated. This thesis describes the techniques for analysis of these antennas both numerically and experimentally. The results of these investigations are contrasted to develop an optimum design. In addition, the automated synthesis of broadband impedance matching networks was accomplished using the Real Frequency Method as well as a modification of this method.

DEDICATION

I would like to dedicate this work to

Jennifer Marie

and my parents,

who have been my inspiration and made this endeavor well worth it.

Thanks.

ACKNOWLEDGEMENTS

The author would like to acknowledge the following contributions:

Professor Raj Mittra, for his orchestration of this project;

Dr. Omar Ramahi, for background research and numerical analyses;

Francois Colomb, for his expertise in the use of the measurement equipment;

Greg Otto, for his help with FORTRAN and programming concepts;

Leisl Little and Jon Veihl, for their related monopole analyses;

Vaughn Betz, John Svigelj, and Rob Wagner, for additional help;

Dr. Amir Boag, for his suggestions on improving the matching program.

TABLE OF CONTENTS

I. INTRODUCTION

A vital concern in antenna design revolves around structure miniaturization. Compact antennas exhibit many positive attributes especially for military vehicle applications. Small structures are much less conspicuous, easier to transport, and can be mounted on vehicles with limited surface area. On the other hand, antennas that are relatively small in terms of wavelength encounter performance difficulties, especially in terms of radiation efficiency and gain. Indeed, the references show that there is a physical limitation to the miniaturization of an antenna [1], yet it is possible to design an antenna with an optimal combination of these parameters. The need for antenna simplicity and durability along with an omnidirectional radiation pattern made the monopole an ideal choice for military applications. Monopole antennas are characteristically narrow band, though, and at low frequencies require a large profile height to perform optimally since resonance occurs when the height measures $\lambda/4$. This makes the design for this application more difficult to realize.

The design of communication antennas for military vehicles presents many challenges. The structure must be sturdy enough for battlefield conditions, reasonably efficient for limited power supplies, omnidirectional, and broadband to allow multiple channel transmission and reception. In addition, the design of a low physical profile is essential to enhance combat survivability by reducing the chances of enemy visual detection. Therefore, the desire to minimize profile height while maximizing the performance of these vehicle antennas was the driving point in this research. Given the desired frequency range, the mission was to design a monopole antenna structure that would radiate omnidirectionally and efficiently yet require as little "real estate" as possible. Vertical height being the prime geometrical criterion, various geometries were modeled using the Numerical Electromagnetic Code (NEC). Structure modifications were then augmented by assorted loading schemes. To accommodate this analysis, a program was generated to extract data from NEC output files for laboratory use. In addition, advances were made with the numerical modeling of experimental phenomena. The

computational analysis led to fabrication and experimentation of acceptable designs to verify antenna characteristics.

Using the HP8510B Network Analyzer in conjunction with two anechoic chambers, a detailed analysis of impedance and radiation was performed for comparison to numerical data. Since some antenna geometries were more easily built and tested in the laboratory than modeled on the computer, physical models alone were used for design evaluation. It was determined that by altering the geometry of a straight vertical monopole, profile height could be minimized while improving impedance characteristics. Resistive loading further enhanced antenna impedance, but radiation efficiency was adversely affected. A combination of appropriate loading and geometry led to antennas that not only maintained an omnidirectional radiation pattern, but also produced energy distributions that were acceptable for mobile ground communication. Multifeed array systems were also analyzed to increase the operational frequency band. By exciting only certain elements in an array of variably spaced nonuniform monopoles, omnidirectional transmission and reception could be accomplished on multiple channels.

Once designs had been satisfactorily completed and verified, both numerically and experimentally, interest turned to the refinement of the antenna/generator interface. The development of impedance matching networks promotes optimum performance for the acceptable designs. The Real Frequency Method (RFM) devised by Carlin [11] was utilized to produce software that orchestrates the design of matching networks for arbitrary antenna structures. Given the measured or simulated input impedance of an antenna over a desired frequency range, user interaction allows engineering control of the matching network response in order to fit design parameters. The program was then modified to simplify the RFM and provide a more complete optimization algorithm. Through the use of user-defined frequency weighting, the computer outputs the components required for a cascaded matching network circuit comprised of reactive components to provide optimum power transfer to the load. The synthesis of these matching networks maximizes the performance of antennas, and by

increasing efficiency, a low profile design becomes more feasible for military vehicle applications and many other monopole antenna systems.

2. COMPUTER MODELING

Computer modeling of antenna structures provides great speed and flexibility in the design process. More specifically, a numerical analysis allows an engineer to quickly examine numerous iterations of geometry and loading schemes without physical model construction. In this research, the Numerical Electromagnetic Code was implemented on a Macintosh IIfx computer to examine antenna models.

2.1 Numerical Electromagnetic Code and Data Extraction

The Numerical Electromagnetic Code (NEC) is a user-oriented software package for the analysis of the electromagnetic response of antennas and basic metal structures. The program uses the numerical solution of integral equations to solve for currents induced on a structure by a specified source [2]. For this research, antenna geometries were input as connected wire segments and evaluated for various frequency ranges. To determine a design's suitability to the military ground communication application, values of input impedance, efficiency, and gain for each antenna model were examined using the NEC software. Since the computation time varied proportionally with the number of wire segments in the model, the electrically small structures of this research were analyzed fairly rapidly.

One inconvenience encountered with the code was the organization of its output data files. NEC arranges all information in a complex tabular form listing after each particular frequency. This makes extraction of relevant data for graphical analysis quite tedious. By writing a program to examine the text files and remove only the desired values, NEC modeling was made much more expedient. The program *NECextract.apl* has been installed in the Electromagnetic Communication Laboratory for retrieval of impedance/efficiency, segment currents, directive gain at a specified frequency, directive or power gain vs. frequency for a specified theta/phi combination, and electric fields. The smaller data files conserved computer memory and made a graphical analysis easy.

2.2 Numerical Electromagnetic Code Discrepancies and Corrections

The value of any numerical code is determined by its ability to predict measured phenomena. The frequency range given for the vehicle application originally spanned from 30 MHz to 450 MHz. In order to accommodate testing equipment (described later), it was necessary to use a scaling factor of 6 to increase the experimental range from 180 MHz to 2.7 GHz. The antenna specifications later dropped to a range of 2 MHz to 30 MHz, which increased the scaling factor to 90 in order to maintain physical dimensions. Since the overall emphasis hinged around minimizing the profile height of the antenna, the monopole was chosen for an assumed "maximum acceptable" vertical height of 0.051m and all other geometries were limited to values less than this height. A linear monopole was the first geometry investigated in order to act as a performance comparison to subsequent trials. Figure 2.1 shows the crucial dimensions for the analytical model. To coordinate the physical experimentation with numerical analysis, structures were entered into the computer with pro-

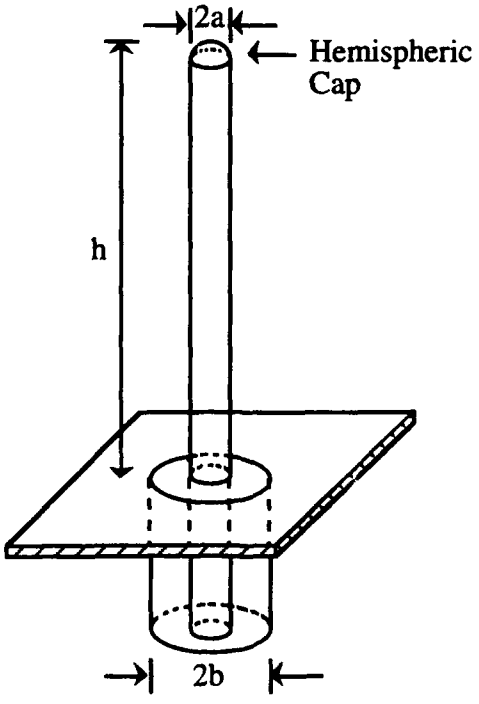

Figure 2.1 Dimensions of a monopole model.

portions similar to the materials available for fabrication. Antenna dimensions were also kept identical to those in the laboratory. Despite this careful modeling, significant errors were encountered when comparing numerical to measured results. Figures 2.2(a) and (b) show the input impedance for a linear monopole over the testing frequency range. The comparison of measured results to those obtained through the use of both NEC and a finite ground plane analysis yielded unaccounted discrepancies. Obviously, the ground plane assumptions were not the cause of the error; therefore, attention turned to other limitations of the codes. Although the programs were unable to model circumferential currents and hemispheric caps on antenna terminations, it was determined that these errors were minor in comparison to the problems encountered with the dimensions of the antenna and its junction with the ground plane.

The first important dimension of the monopole was its height or wire length. Each antenna model was comprised of a series of wires that were in turn, divided into segments. The size of the model segmentation limited the accuracy of the numerical code. The NEC User's Manual states "The main electrical consideration is segment length Δ relative to the wavelength λ. For accuracy, segment length should remain below 0.1 λ and above 10^{-3} λ." Along with the segmentation, overall monopole length was also a factor. NEC experienced difficulty in analyzing antennas at frequencies at which monopole length became significantly small in terms of wavelength. In this analysis, the output files exhibited impedance discontinuities and negative efficiencies with folded geometries when the total conductor length decreased below $\lambda/4$, i.e. 500 MHz. Another important dimension in the numerical model was the ratio of wire radius to segment length. NEC documentation recommended the use of an extended thin-wire kernel which allowed for segments to be as short as one-half radius. Therefore, segment lengths were confined to approximately 0.005 m to meet these requirements. Since rapid changes in wire radius between adjacent segments caused impedance mismatches, structure radii was kept constant throughout the models. It will be shown later though, that wire discontinuities were essential to the accurate modeling of lumped loads.

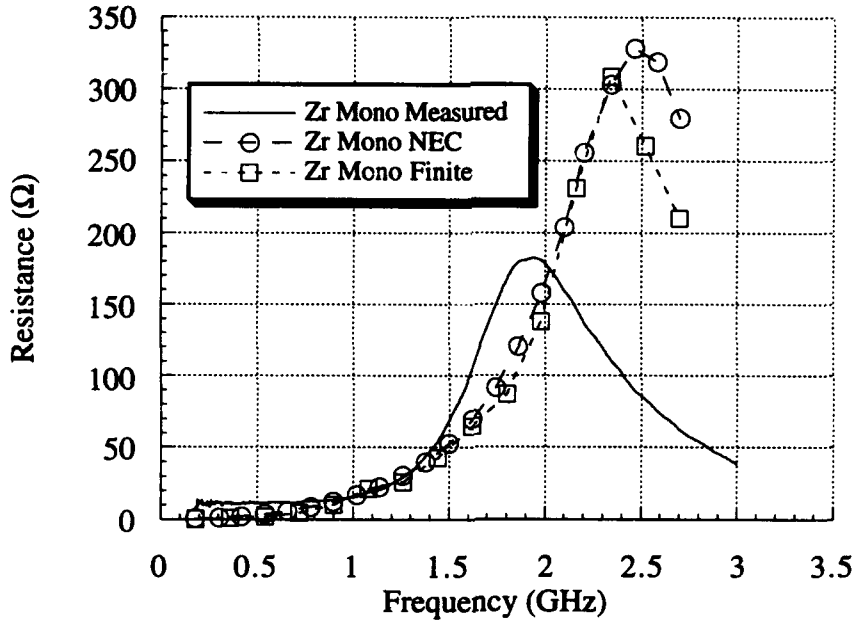

(a)

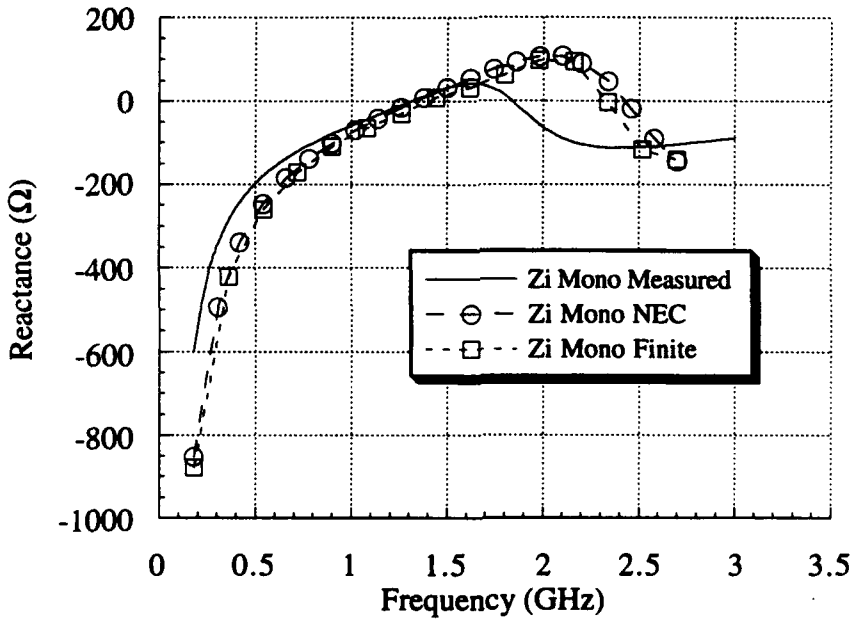

(b)

Figure 2.2 Comparison of measured impedance to NEC and finite ground plane analyses of a 5.1 cm linear monopole: (a) resistance (b) reactance.

In addition to these lengths, the radii labeled *a* and *b* in Figure 2.1 have a significant effect on the input impedance of a monopole. King and Hartig experimented with the effects of these dimensions [3]. Ideally, the wire radius should be infinitesimal to negate the presence of circumferential currents. However, in practice, wire radii must be finite; and as wire radius increases, the peak impedance amplitudes and resonant frequencies decrease as shown in Figures 2.3(a) and (b). King's results were repeated at the University of Illinois for varying wire radii, and can be compared in Figures 2.4(a) and (b). For fabrication purposes, a wire radius of 0.00138 m was selected for the models due to its compatibility with the type N connector coaxial center conductor size. This put the diameter/wavelength ratio of these experiments in King's "moderately thick" category which shifted the impedance curves as expected. For the linear monopole it was noted that the resonance frequency calculated based on a $\lambda/4$ height was 160 MHz greater than the value measured in the laboratory. King's graph shows that measured resonance was 22.2 MHz less than the ideal dipole value. Using a scaling factor of 5 to match frequency ranges, King's results would give a difference of approximately 111 MHz which is similar to the University of Illinois results. This fact did not, however, explain the vast differences between amplitudes and antiresonant points for the measured and calculated values seen in Figure 2.2. In order to explain this phenomenon, it was necessary to look at the ratio of *b/a* and the resulting influence of the connector. Once again, King had previously analyzed the effects of the magnetic frill created by the junction of the connector with the ground plane. Figure 2.5 from The Theory of Linear Antennas [3] demonstrates the influence of the parasitic capacitance resulting from a finite gap between the antenna and the ground plane. Note that as the value of K changes (indicating a shunt capacitance load), the impedance curves follow the dashed envelope. As *b/a* -> 1, K ->0, and the impedance approaches a quantity characteristic exclusively of the antenna [3]. NEC assumes this dirac delta gap at the coaxial junction, but the dimensions of a type N connector are more complicated as seen in Figure 2.6. The finite ring of dielectric at the junction in Figure 2.6(b) creates a phase lag in the currents which induce a parasitic capacitance on the im-

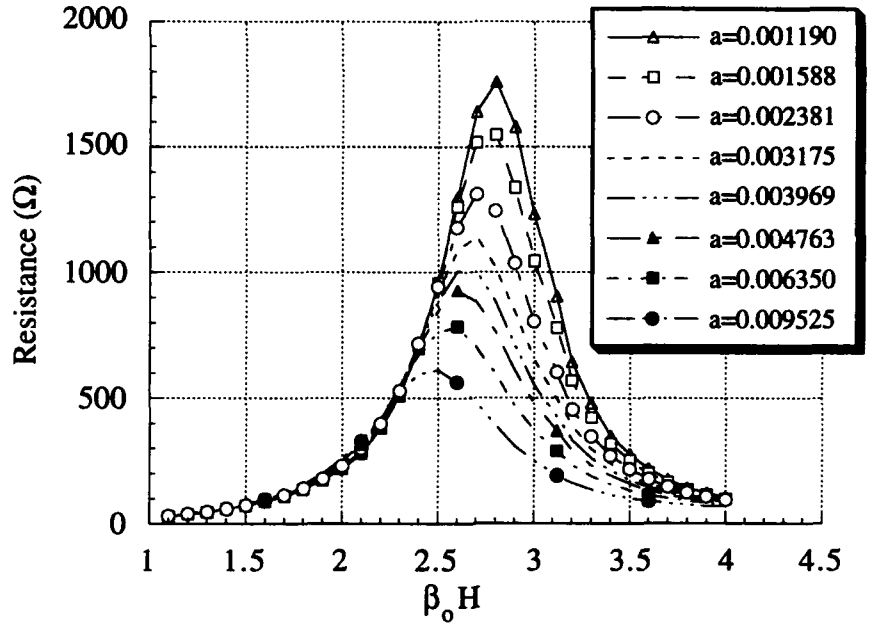

(a)

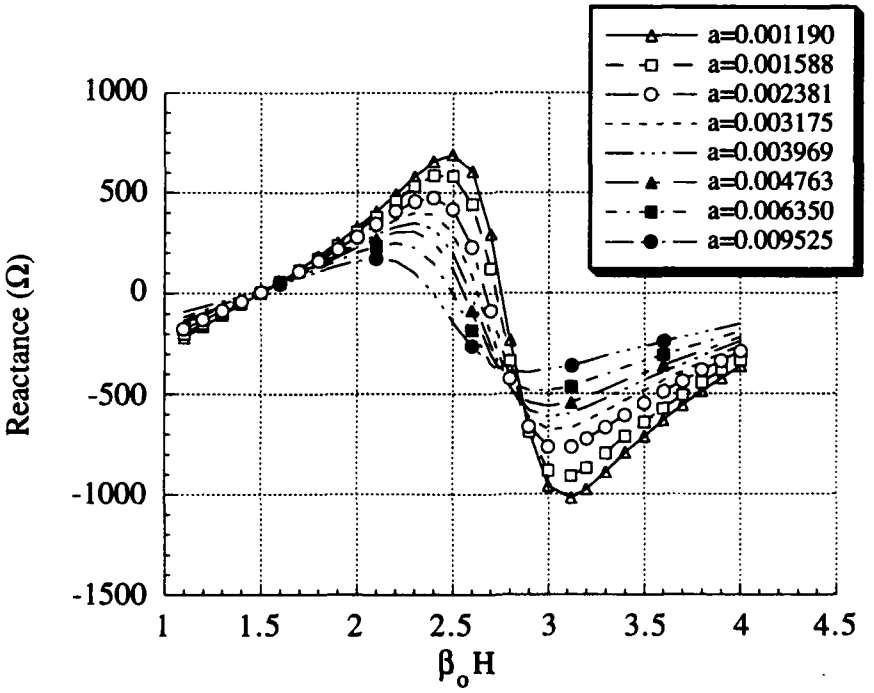

(b)

Figure 2.3 Measured impedance from King, The Theory of Linear Antennas for various radii monopoles: (a) resistance (b) reactance [3].

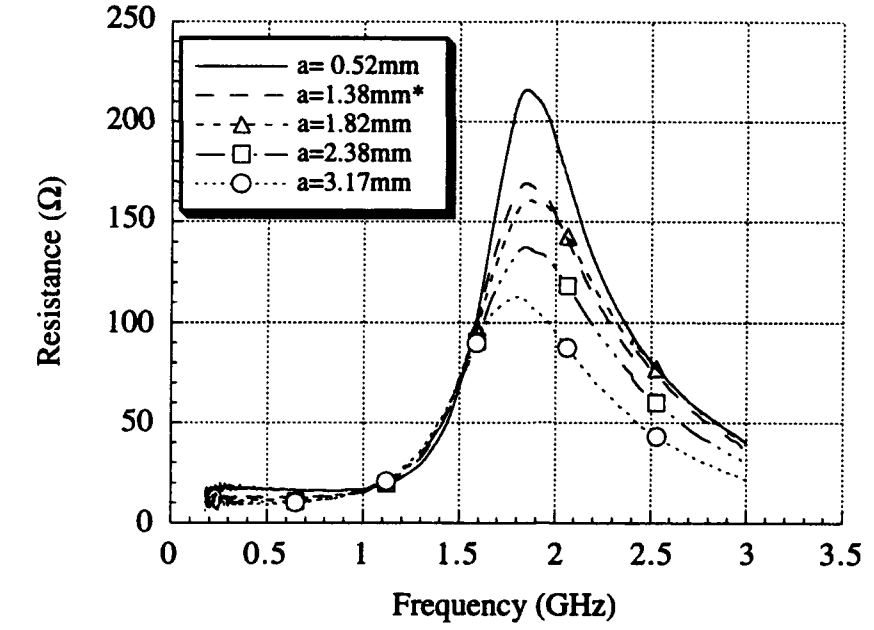

(a)

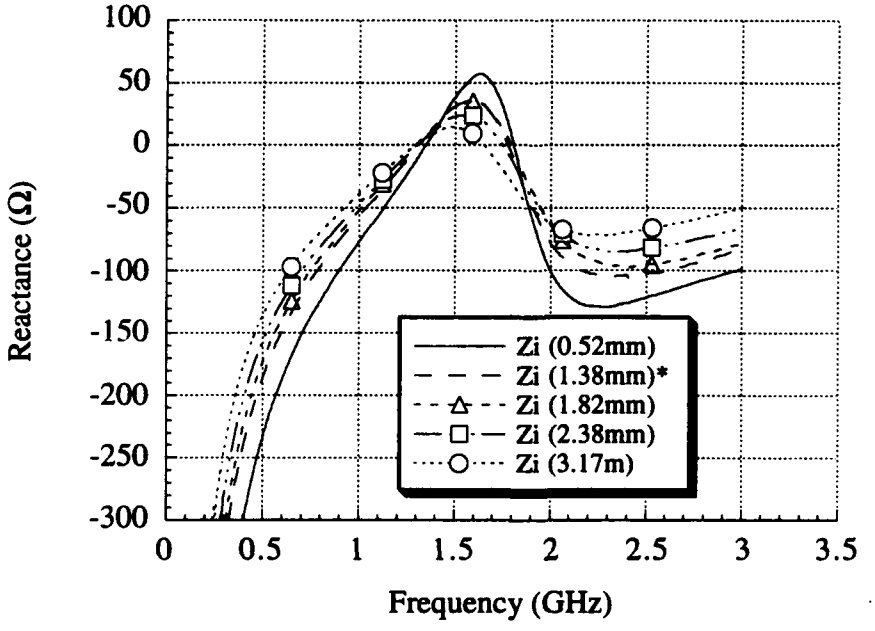

(b)

Figure 2.4 Impedance measured at the University of Illinois for various radii monopoles: (a) resistance (b) reactance.

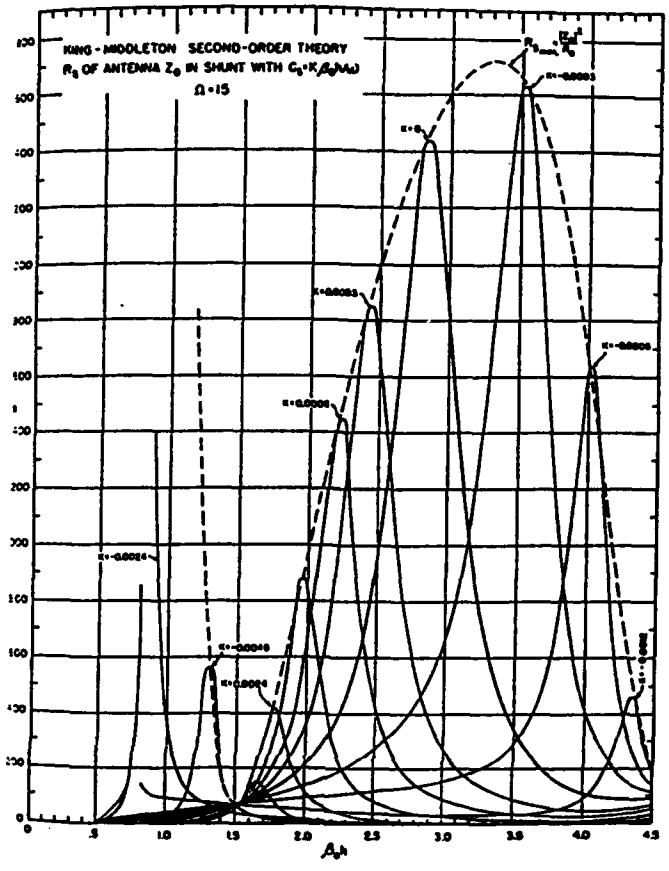

Figure 2.5. Effect of parasitic capacitance from King [3].

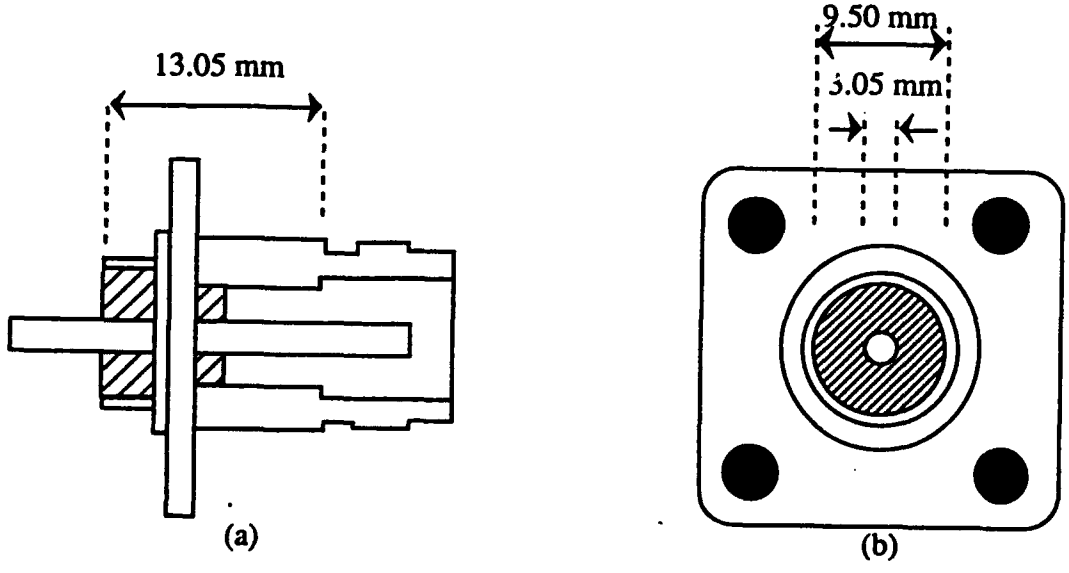

Figure 2.6 Type N connector schematic: (a) side view (b) front view.

pedance plots. The ratio of radii (*b/a*) determines the phase lag, and in type N connectors this ratio is significant with a value of 5. Although the finite ground plane code is currently being revised to account for this effect, in order to implement a correction in NEC, it was necessary to adjust the input models accordingly.

2.3 Modification Results

The addition of a capacitive load at the base of the antenna model significantly improved the impedances as seen in Figures 2.7(a) and (b) which compare the numerical models previously shown to the modified NEC model and the measured result for the monopole. A 0.15 pF point load was connected from the top of the feed segment at the base of the model to a point 0.005 m from the base to emulate the radius of the ring. The loading wire radius was kept the same as for the structure to prevent discontinuities. This load was then implemented on subsequent NEC models with more complicated geometries whose results are seen in Chapter 3. It was interesting to note that the parasitic capacitance and wire radius significantly affected amplitude and antiresonant points, but left the resonant points unchanged.

2.4 Loading Model Considerations

The final modeling consideration dealt with the addition of lumped loads used for broadbanding the geometries. NEC has the ability to model a lumped load as either a point impedance at a segment center or a distributed load along a combination of segments. Point loading worked well for reactive components, but the simplicity of resistive loads facilitated the user of the distributed type. Since the characteristics of load components vary with frequency, especially at high frequencies where these tests occurred, the components themselves were analyzed for operating characteristics. Figure 2.8 shows the reactance performance of two capacitors from the University of Illinois engineering stores over the desired frequency range (the resistances of the components were negligible). Notice that the components become self-resonant at approximately 1 GHz and 2.2 GHz. Because of these variations and the unavail-

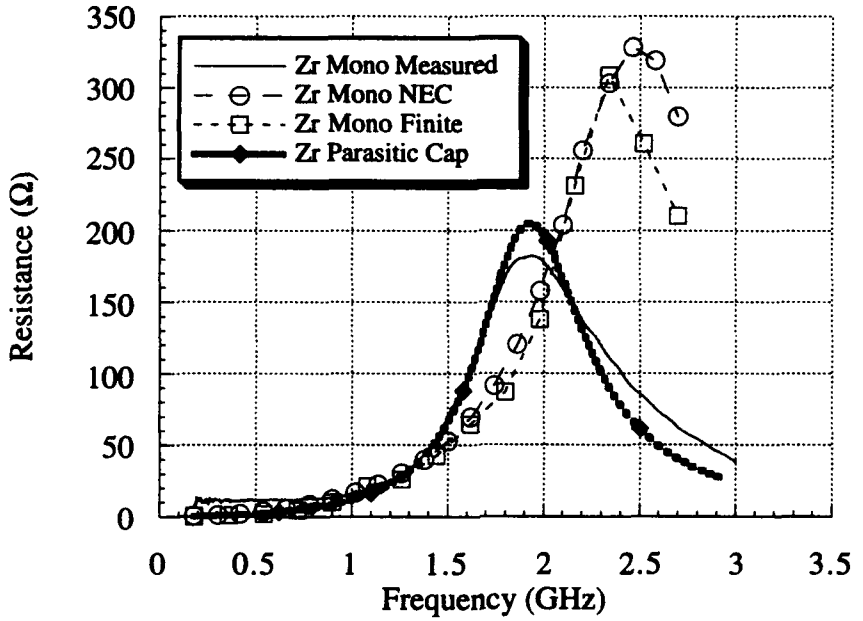

(a)

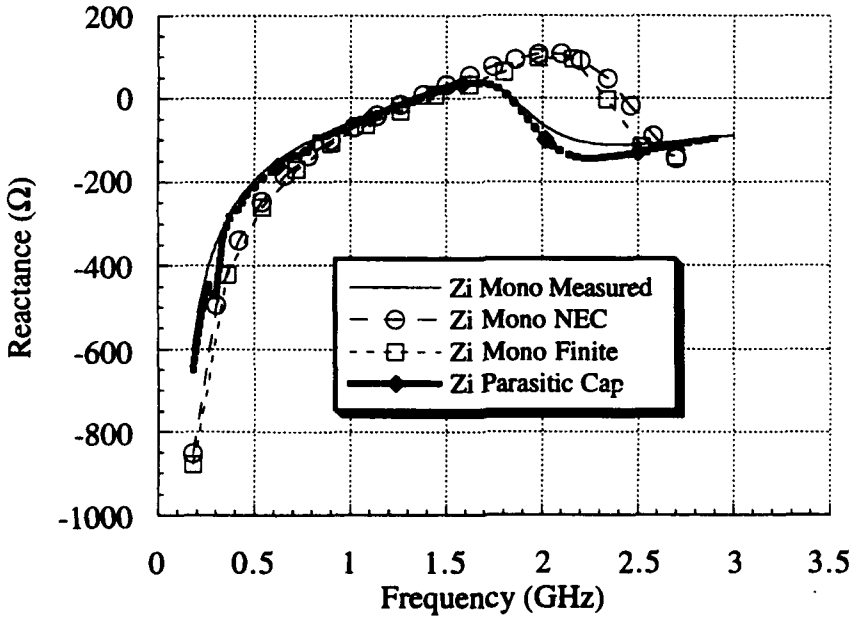

(b)

Figure 2.7 Comparison of monopole impedance, including results from the parasitic capacitance modification: (a) resistance (b) reactance.

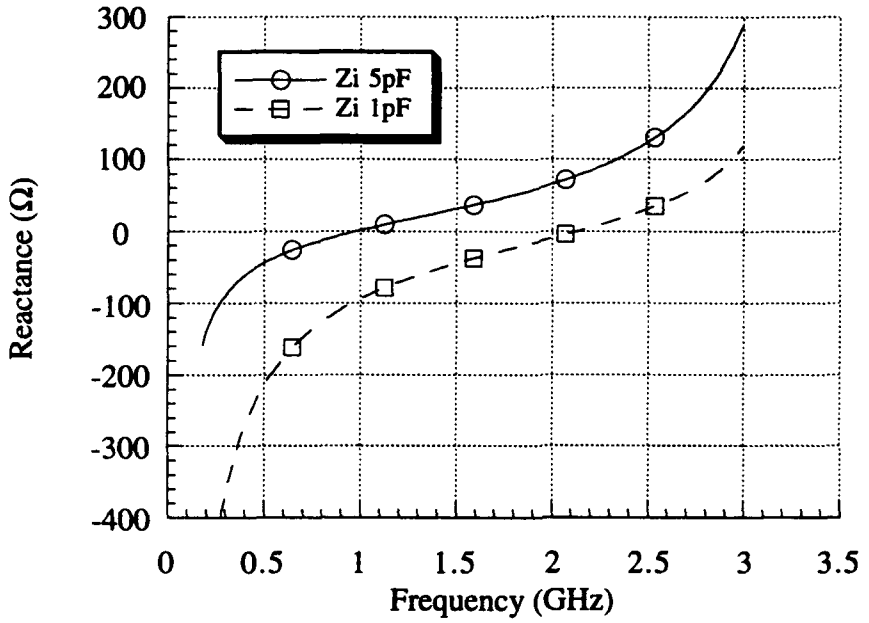

Figure 2.8 Measured reactance of disk capacitors.

ability of high frequency reactive components (e.g., chip capacitors), lumped reactive loading was avoided although some numerical analysis has been completed. This prompted research into sleeve loading (discussed later) also covered in the literature [4].

Despite reactive loading difficulties, lumped resistive loading produced promising results, and through detailed geometric modeling with distributed loading, NEC was able to simulate the high frequency characteristics of resistive components in the antenna models. Figure 2.9 illustrates the measured dimensions used in the NEC analysis for a 1/4 W resistor.

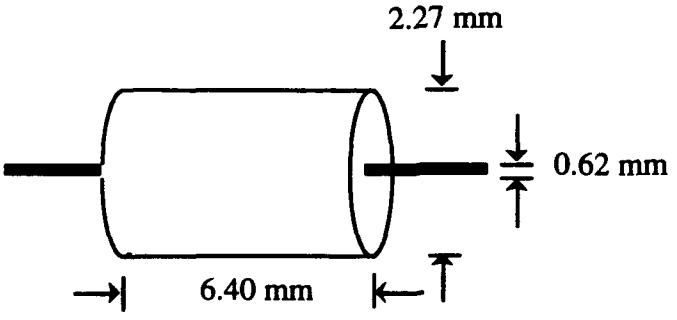

Figure 2.9. NEC lumped load dimensions.

Although in theory resistor characteristics should be frequency independent, at high frequencies, component construction becomes important to the model. For example, depending on the length of the component leads, a parasitic inductance can be calculated using (2.1) [5].

$$L = \frac{\mu_0}{2\pi}\left(\frac{1}{2} - \ln a\right) \tag{2.1}$$

In addition to this inductance, the lead contacts produce a parasitic capacitance which makes the model more difficult to simulate. In order to understand the response of the resistor at our test frequency range, the component's impedance was measured in the laboratory and compared to the same configuration on NEC. Figure 2.10 shows the results of the comparison. The measured values for both resistance and reactance appear relatively stable throughout the frequency range. However, although the NEC analysis seems to converge towards the response for higher frequencies, the large errors show the limitation of NEC's ability to approximate very small structures (i.e., the resistor mounted to a ground plane) and the limit-

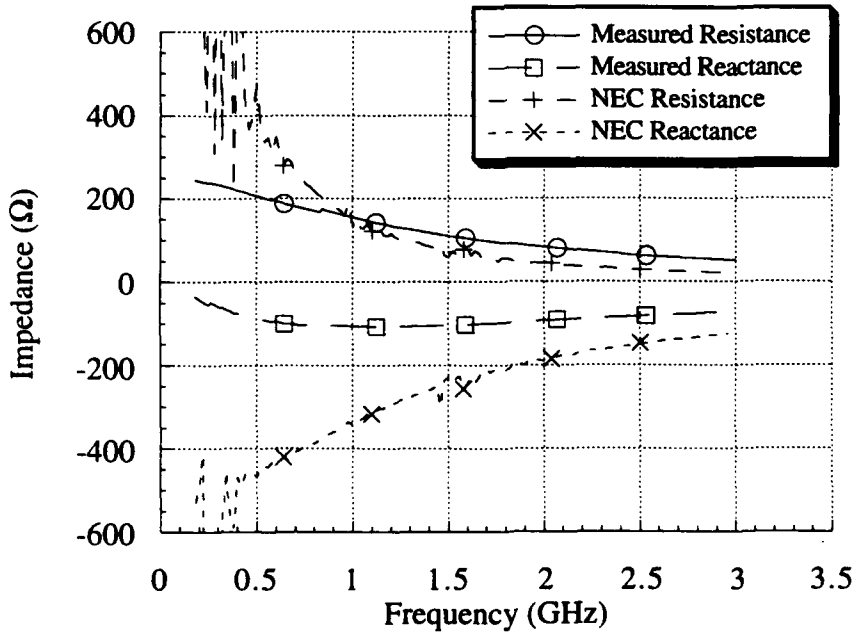

Figure 2.10 Measured and NEC impedance of a 240 Ω resistor.

ation of the magnetic frill approximation. Despite these differences, the use of actual wire radii as well as distributed loading across the resistive segments produced an accurate simulation for the numerical model. The results from more complicated resistively loaded antennas will be seen later.

3. FABRICATION AND EXPERIMENTATION

3.1 Design Fabrication

In order to properly verify the results of the numerical analysis, the NEC models were fabricated for experimentation in the laboratory. In some cases, due to the complexity of a model and computation time, building and measuring an antenna were the most efficient methods to evaluate the design. One example of this came from the analysis of sleeve structures. Both grounded and fed sleeves were experimented with, and in each case, sleeves had to be numerically represented by a cylinder comprised of wire segments. The resolution of the sleeve was dependent on the number of vertical segments present , and the addition of horizontal segments was necessary to model circumferential currents. Since this led to complex numerical representations, and NEC analysis time is proportional to the number of segments used, computation grew to unacceptable levels. Even without these difficulties, experimental analysis remains the only method to determine the actual characteristics of a design. As seen in Chapter 1, computer analysis must be able to predict natural phenomena; therefore, differences between our computational and measured results necessitated the correction of our numerical model to include the magnetic frill.

All models were attached to the same circular aluminum ground plane. Antenna structures were comprised of similar linear segments of wire. The method of fabrication was standardized between the different geometries. Wire segments were bonded using Kester solid wire solder and a paste flux for strength and durability. Grounded components were connected to the ground plane using copper tape. By choosing a standard structure wire radii of 0.00138 m, the antenna model size matched the radius of the connector's coaxial center feed. By filing the junctions at the feed, structure discontinuities were avoided to minimize energy reflections. This wire size also allowed sufficient space to implement lumped loading using the method shown in Figure 3.1. The antenna wire was bored out to enable soldering of the lumped component leads. To improve the structural integrity, a dielectric plexiglass sheath was also

drilled out to the size of the conductor wire and applied to the severed section of the antenna. The presence of the sheath was tested and found to have a negligible effect on antenna impedance and radiation characteristics. By varying the radius of the sheath and the volume of the loading station, multiple lumped loads could be implemented with this mechanism. One example of multiple component loading is addition of tank circuits for current choking.

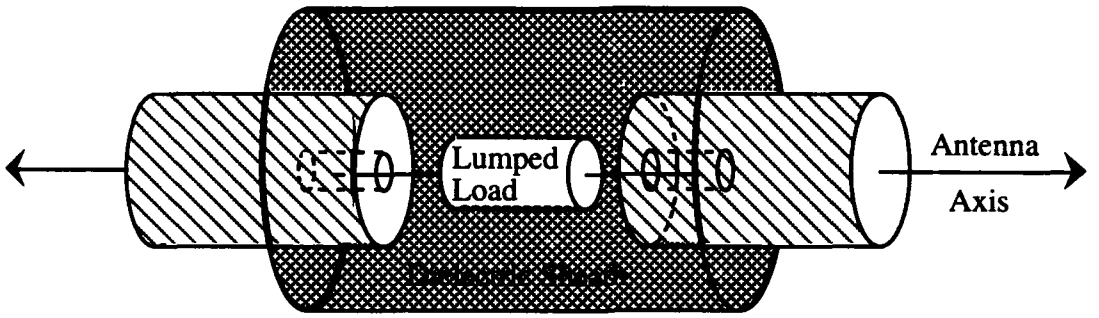

Figure 3.1 Lumped load implementation technique.

Structure dimensions were driven by the frequencies desired. The frequency range of interest originally spanned from 30 MHz to 450 MHz. Models were scaled by a factor of 6 to increase the range from 180 MHz to 3 GHz. This increase in frequency was necessary not only for the network analyzer, but also for the measurement facilities described later. Some analysis was necessary on structures down to 2 MHz, which indicated that the models would be scaled by a factor of 90; however, the frequency range would only span to approximately 33 MHz.

3.2 Measurement Equipment

The experimental portion of the investigation was limited by the size of the measurement facilities. The input impedance and radiation patterns of our test antenna configurations were evaluated by the HP8510B Network Analyzer, which has a large testing frequency range. For the lower frequencies, the limits of the S-parameter test set were stretched, but a comparison of the results was good throughout the frequency range. The size of the two anechoic chambers used for impedance and pattern measurements limited our testing range.

The network analyzer was calibrated using type N standards for a 7 mm, 50 Ω coaxial low-loss connection cable. A three-term calibration was conducted using a Hewlett-Packard open, short, and broadband 50 Ω load. Although the calibration sequence was menu driven, some subtleties existed. One dealt with the definition of the load type which is determined "male" or "female" based on the connector *accepting* the load. Another deals with the definition of the measurement reference plane. Calibration using these standards sets the reference plane at the point where the type N connector mates with the low-loss cable. Referring back to Figure 2.6(a), which represents the side view of a type N connector, notice the difference between the reference plane established by the calibration standards and the reference plane for the antenna (which is defined by the location of the ground plane). This made it necessary to induce an electrical delay to account for the signal's round trip across this distance. By using a type N connector configured as a short, the geometric difficulties were solved with the addition of a time delay of approximately 72 ps.

Information from the network analyzer could be plotted directly from the device in many formats (e.g., Smith chart and log mag). For a more detailed analysis, information was transferred to a Macintosh IIfx computer where it was then loaded into graphical evaluation software such as Kaleidagraph. Programs for removing information from far-field pattern measurements had already been written for the laboratory. These programs remove pattern data for a frequency determined by the user. Additional information about the network analyzer can be found in the references [6].

3.2.1 Impedance measurements

Impedance measurements were performed using a one-port S_{11} calibration. To minimize the effects of noise, each antenna model was measured while mounted in the small anechoic chamber shown in Figure 3.2. "The box" was designed to accept a circular ground plane with a 0.46 m radius similar to the one mentioned earlier. The chamber itself was constructed of wood (with the exception of one aluminum wall serving as a ground plane) with

1.83 m sides on the square faces and a 0.61 m depth. Each nonmetallic face of the chamber had 0.2 m of styrofoam installed to surround the radiating portion of the test location. The circular plane, which was positioned flush with the chamber's aluminum wall, effectively increased the ground plane to a square with 1.66 m sides (1.83 m sides when including the aluminum that resides under the styrofoam absorber). As stated earlier, by scaling the models, the lowest testing frequency was 180 MHz. This meant that the ground plane measured approximately 1.0 λ x 1.0 λ at the lowest testing frequency which gives more confidence to our measured results.

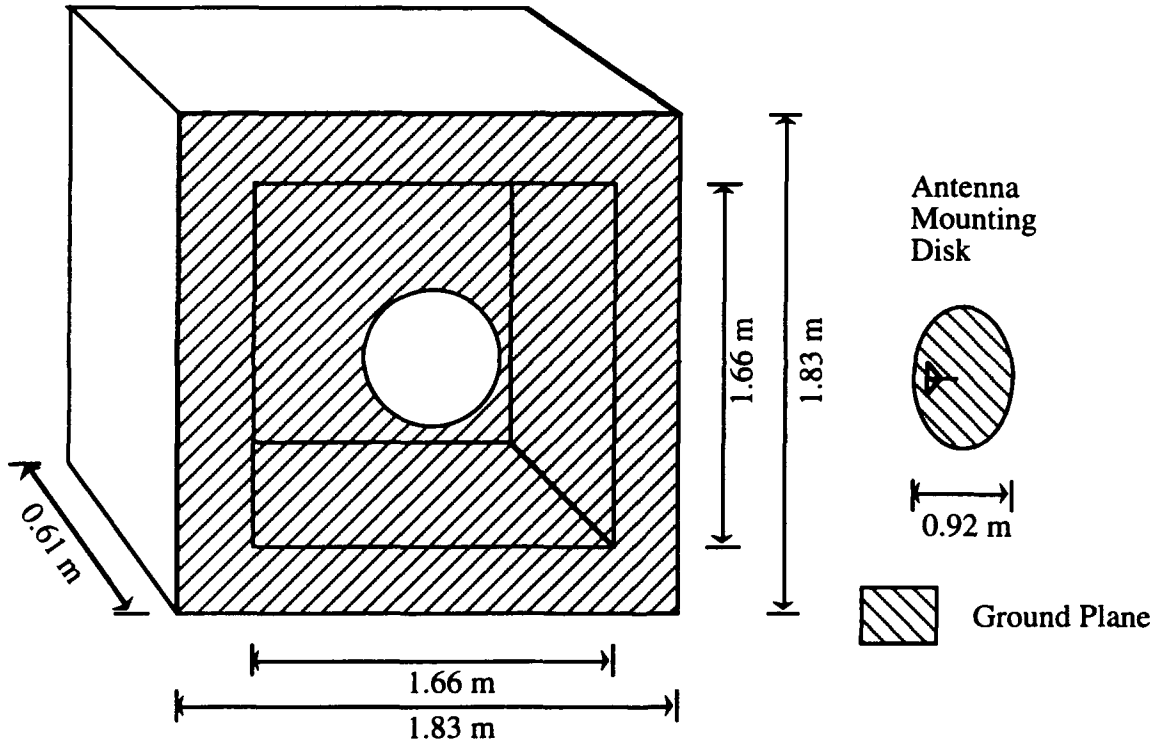

Figure 3.2 Anechoic chamber for impedance measurements.

3.2.2 Pattern measurements

Although pattern measurements were not conducted as often as those for impedance, they were used to determine the omnidirectionality of a design's radiation. A diagram of the anechoic chamber can be found in Figure 3.3, which is oriented from the receiver end to the testing location and alignment wall. The chamber measured 3.66 m x 3.66 m x 15.24 m and

was configured to allow the test antenna to be fed at a rotating test location in the center of the chamber. All walls were lined with a cone-shaped absorber, and equipment for antenna feeding and power controls was concealed beneath the chamber floor. Following the steps found in the pattern reference guide [7], the receiving antenna was first aligned with its stand, then with the chamber, and finally, with the test antenna. The circular ground plane was placed in a wooden frame which was bolted to the rotating mechanism in the center of the chamber. This configuration allowed the antenna to be rotated from θ=-90° to +90° [pattern range nomenclature for θ] for a particular value of ϕ. The value of ϕ could be changed by rotating the circular ground plane within its wooden frame, but ϕ cut patterns were limited to numerical analysis. Feed lines run from the analyzer system through an amplifier to the test antenna. The signal was then received at the near end of the chamber with a receiving horn that was computer controlled and rotated for measuring both vertical and horizontal polarizations. Since we were dealing with monopole antennas, we were primarily concerned with the field in the θ direction, or vertical polarization.

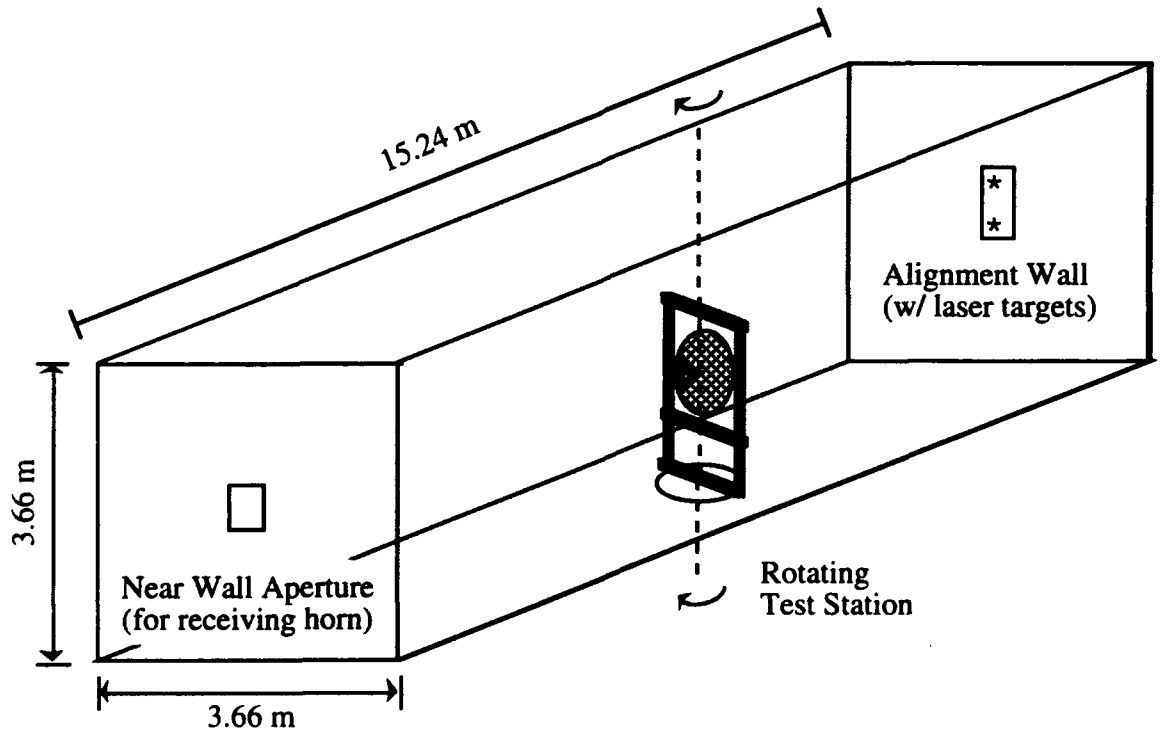

Figure 3.3 Anechoic chamber for pattern measurements.

For this measurement, the analyzer was calibrated with a thru-cal for measurement of S_{21}. The chamber was somewhat limited to frequencies at or above 2 GHz due to physical size and power considerations. For frequencies below 2 GHz, the limited cross-sectional area resulted in energy reflection that degraded the measurement. Also, in order to measure S_{21} without changing the amplifier equipment, the input power had to be decreased to prevent pattern tainting by higher-order harmonics. The dimensions of the chamber dictated that pattern measurements near the horizon (relative to the ground plane) experienced less reflection since the large part of the chamber is aligned with a monopole pattern maximum. On the other hand, fringing from the finite ground plane becomes a factor at these angles. The largest problems occur when the test antenna is rotated to $\theta=0^o$, when the reflections from the chamber walls cause ringing in the monopole pattern.

3.2.3 Current measurement (design only)

Although the design was never implemented, plans were drawn up for a device used to measure currents along the physical structure of an antenna. The device shown in Figure 3.4 uses a probe with a vertically oriented receiving wire to measure E_θ in the near field which is proportional to the longitudinal current. By setting up the network analyzer for two-port measurements, the field at the test location could be measured by viewing S_{21}. The probe would be mounted on a mobile arm, which is, in turn, connected to a dielectric stand to avoid electromagnetic interaction. By moving the probe along the structure, changes in the near field (and therefore, current) could be determined. This type of measurement could be helpful to support numerical analysis, or analyze coupling on structures that are not well-suited to analytic modeling.

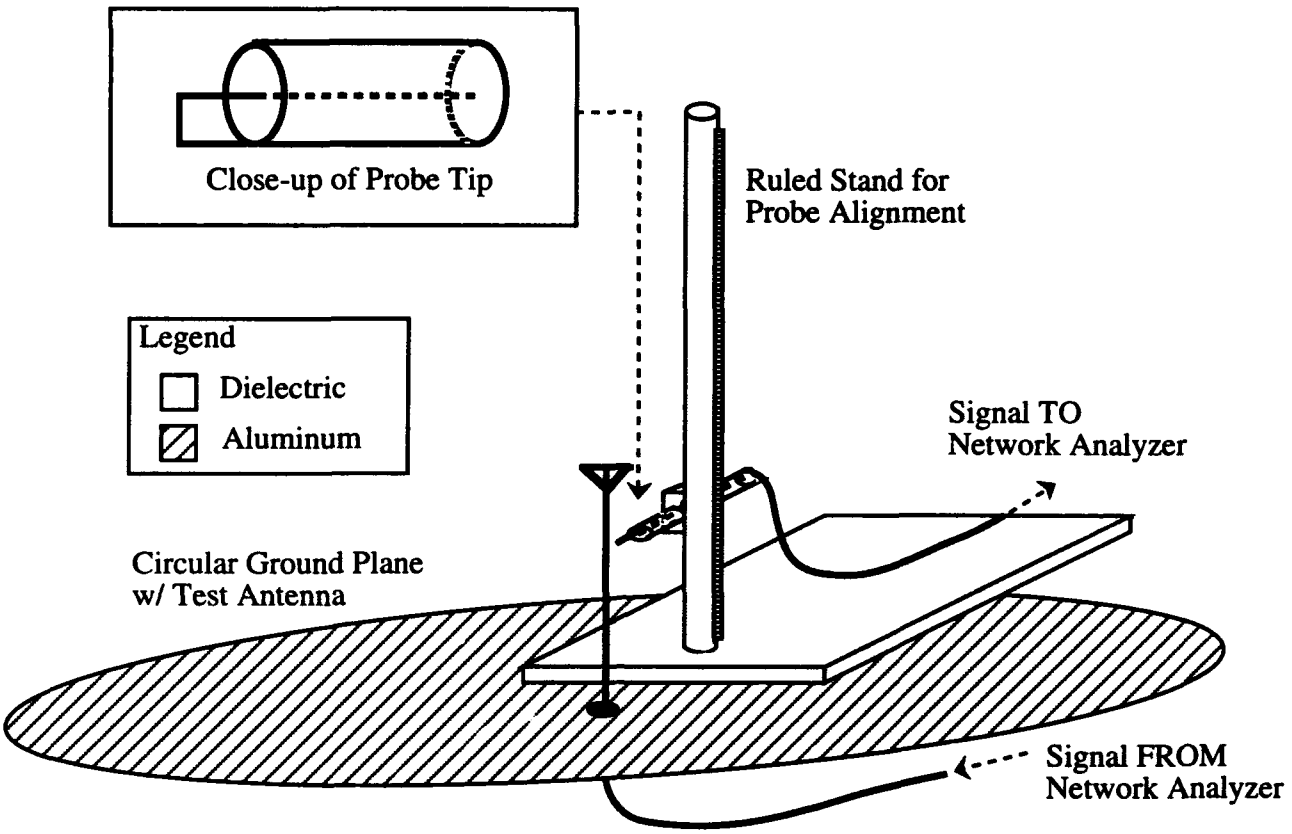

Figure 3.4 Design for current measurement device.

4. LOW PROFILE BROADBANDING TECHNIQUES

4.1 Geometry

The impedance results for a linear monopole were seen previously. When operating frequencies are as low as 2 MHz, as in our military vehicle application, resonance occurs when a linear monopole's length is approximately 37.5 m, which corresponds to the $\lambda/4$ criterion. Obviously, this would be unacceptable in a wartime environment since the antenna would not only be quite immobile, it would also be terribly conspicuous to the enemy. By decreasing the profile height, the antenna became more combat survivable and easier to implement on a weapon system; however, the low frequency characteristics decreased accordingly. Therefore, the objective of geometry alteration was to increase the length and volume of the radiating structure while minimizing height. With this in mind, the limiting vertical height was set to 5.1 cm and geometry modification was attempted to improve the broadband impedance characteristics. The 5.1 cm monopole had a $\lambda/4$ resonant point at 1.47 GHz, which is towards the high end of the 180 MHz to 3 GHz band. This meant that radiation for the lower frequencies suffers. Changing the geometry must not only lower this resonant frequency, it must also be able to produce an omnidirectional far-field pattern throughout the frequency band. This quality is important since the primary use for the antenna revolves around mobile vehicle communication where most of the fields should remain relatively close to the horizon without significant loss to higher elevations. Geometry alone controls the minimization of profile height, but other mechanisms were necessary to avoid sacrificing other antenna parameters. The structure also plays a major role in determining the directionality of the far-field patterns.

4.1.1 "T" geometry

The first geometry alteration augmented the linear monopole by adding a horizontal piece across the top. Figures 4.1(a) and (b) show the dimensions of the linear monopole and

the "T" geometry variation. Although this design increased the effective length of the monopole, the impedance was not significantly improved as Figures 4.2(a) and (b) demonstrate. The added conductor surface helped the low frequency impedance match, but for higher frequencies, the reactance excursions were more intense. In addition, current flowing in a horizontal direction does not improve radiation in the vertical plane which is desired for the received signal. Beyond this, since a monopole conductor produces a pattern with a null at the tip, the T configuration generated a pattern that contained nulls along the transmission direction; therefore, the design was not considered acceptable.

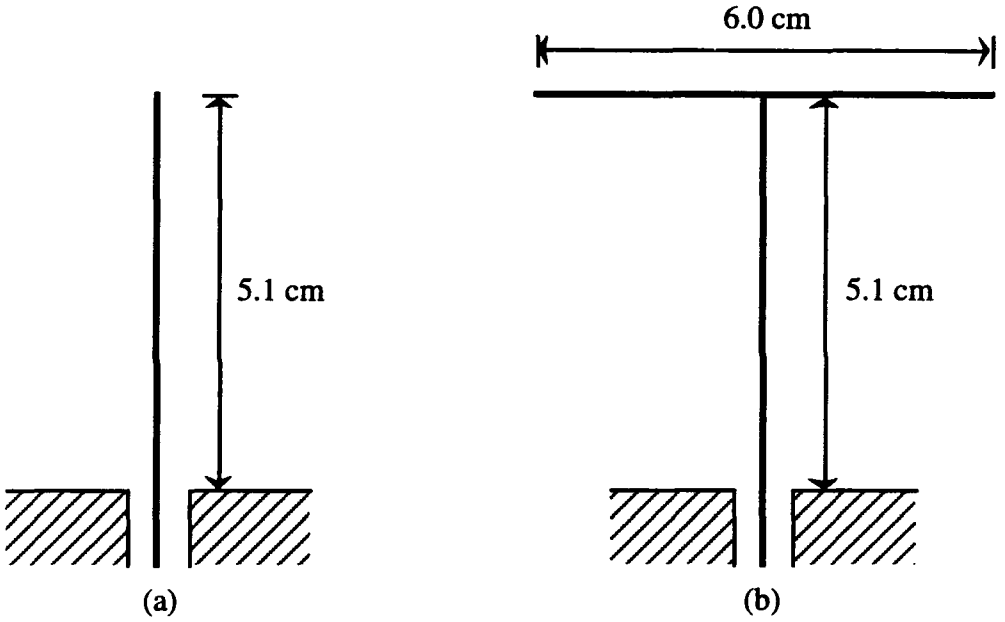

Figure 4.1 (a) Linear monopole (b) "T" configuration

4.1.2 2D and 3D kite geometries

The "Kite" Geometries, so-called due to their distinctive shape shown in Figure 4.3, were merely variations of the linear monopole which included additional conducting material. In the 2D case, arms are added to the structure in one plane. The 3D case combines arms in two planes giving a more universally symmetric appearance. The reasoning behind this geometry was to increase the amount of conductor while keeping the fields omnidirectional and oriented in the vertical plane. The kite geometry follows the concept of a sparse conical mono-

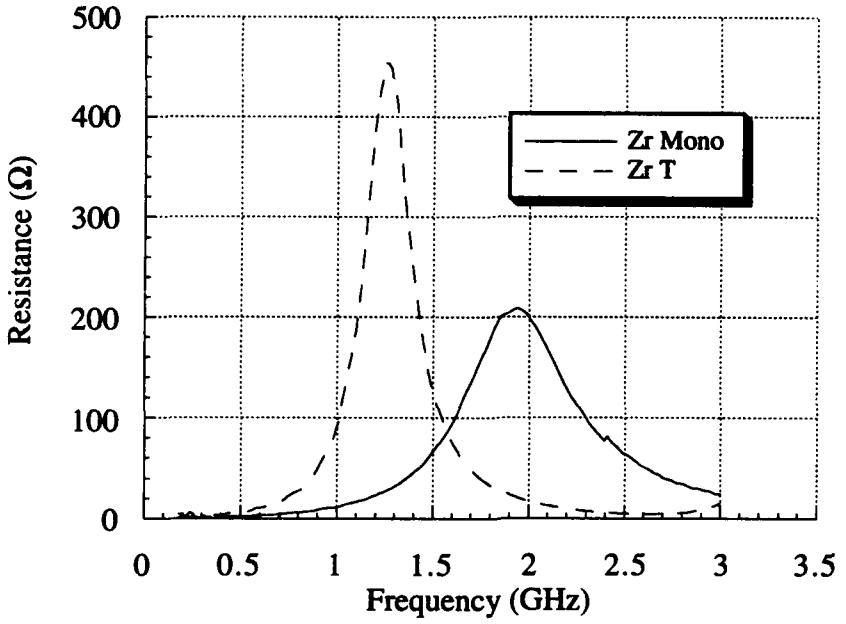

(a)

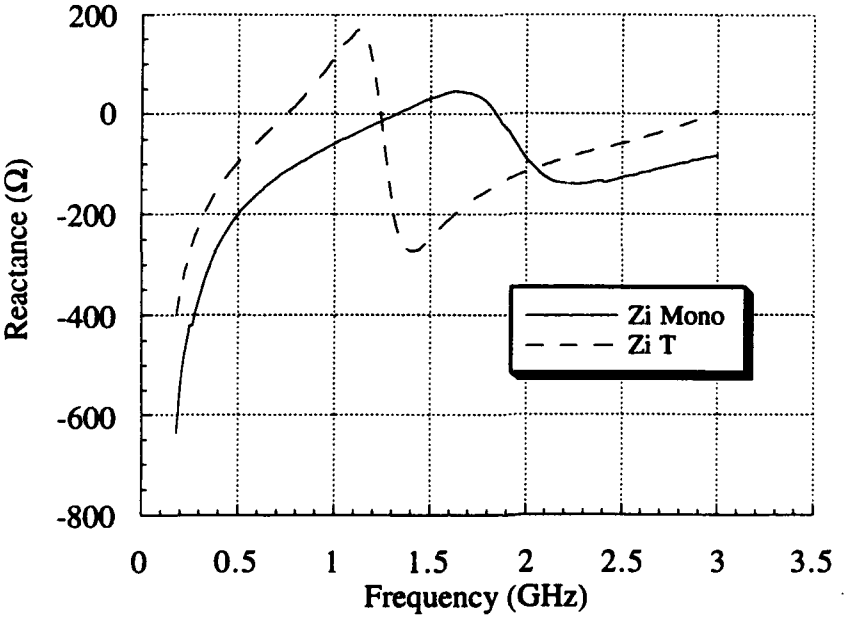

(b)

Figure 4.2 Impedance comparison of linear and "T" monopoles:
(a) resistance (b) reactance.

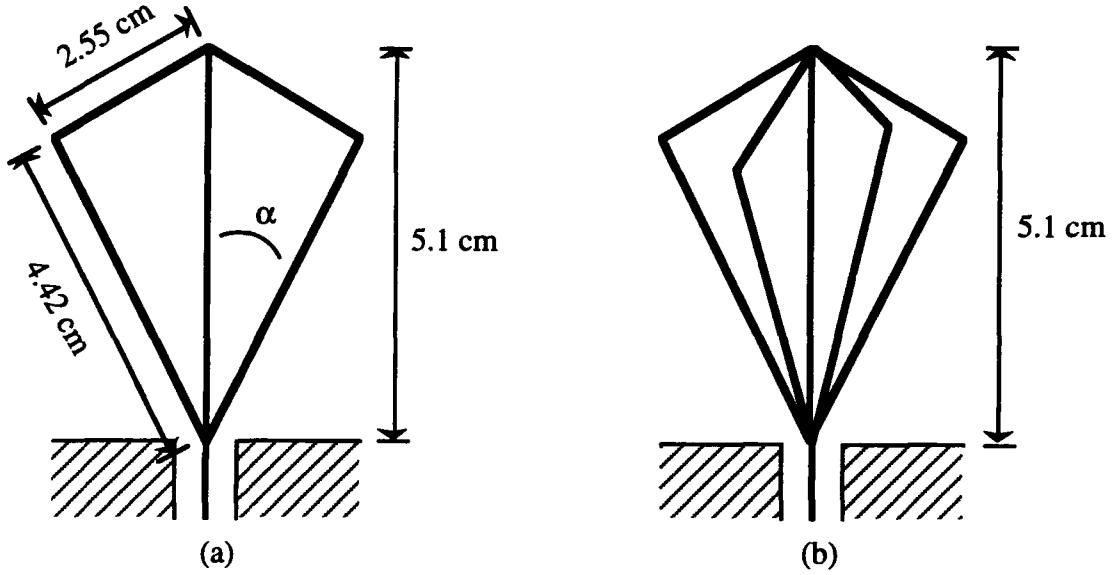

Figure 4.3 (a) 2D and (b) 3D "kite" antenna configurations.

pole. In theory, an infinite conical monopole antenna is frequency independent while a truncated cone's frequency range is dependent on its size. The vertical height of the structure is not the only important dimension; the cone angle also affects its performance. As the angle α increases for the cone, the impedance variations decrease since less coupling occurs between the arms [8]. Although the complexity of construction did not allow experimentation of the angular phenomenon, a numerical analysis was conducted for the two-dimensional case and the results are shown in Figure 4.4. In this study, α varies from 15^{o} to 30^{o} and 45^{o} and results match those expected. The impedances plotted in Figure 4.5 show that the increased volume of the kite geometry resulted in significant reactance improvement for the low-frequency end (from approximately -600 Ω to around -350 Ω); however, in the upper portion of the frequency range there was little difference between the kite and linear monopole.

4.1.3 Gamma geometry

It would appear that to increase conductor length without affecting the profile height, a horizontal wire would be ideal. This is not the case however, because a horizontal conductor would act as a transmission line which would be an inefficient radiator, and would not promote

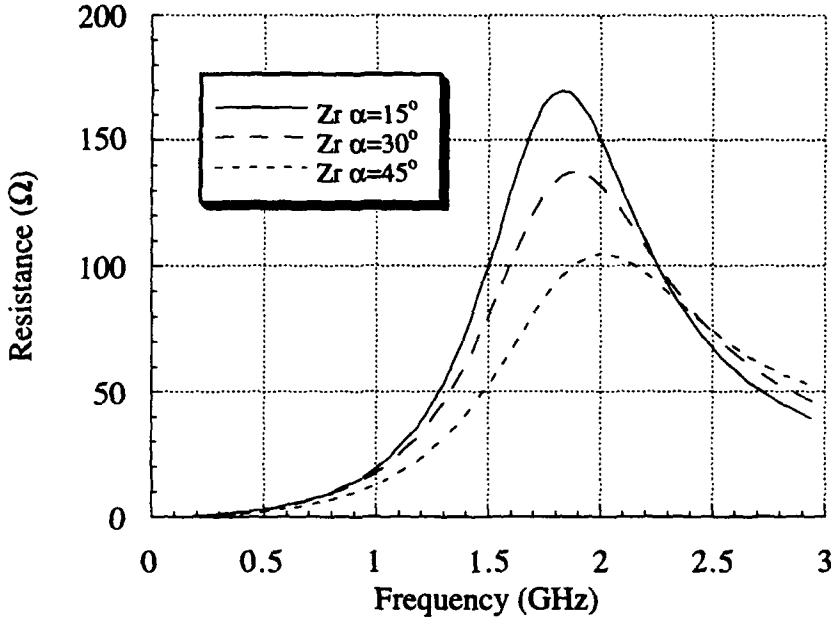

(a)

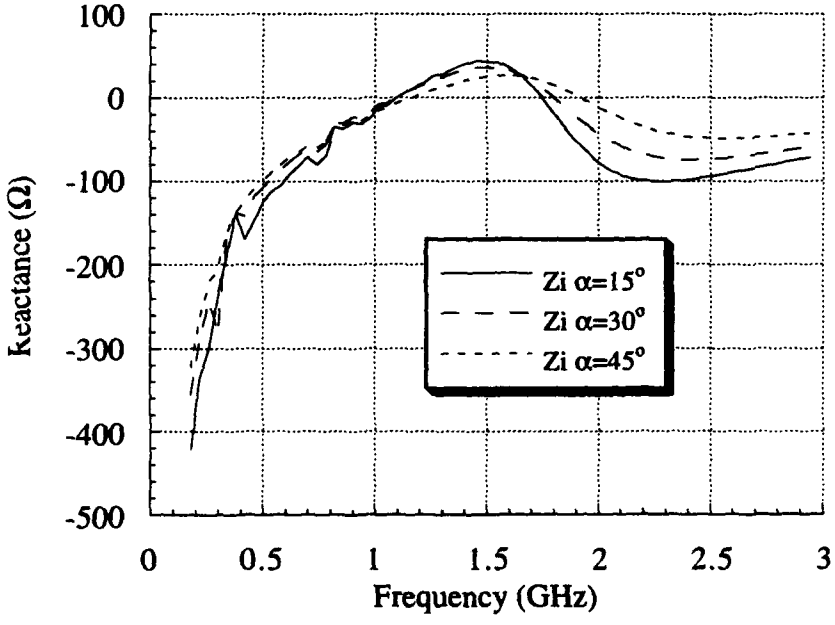

(b)

Figure 4.4 Impedance of 2D kite geometry with varying α:
(a) resistance (b) reactance.

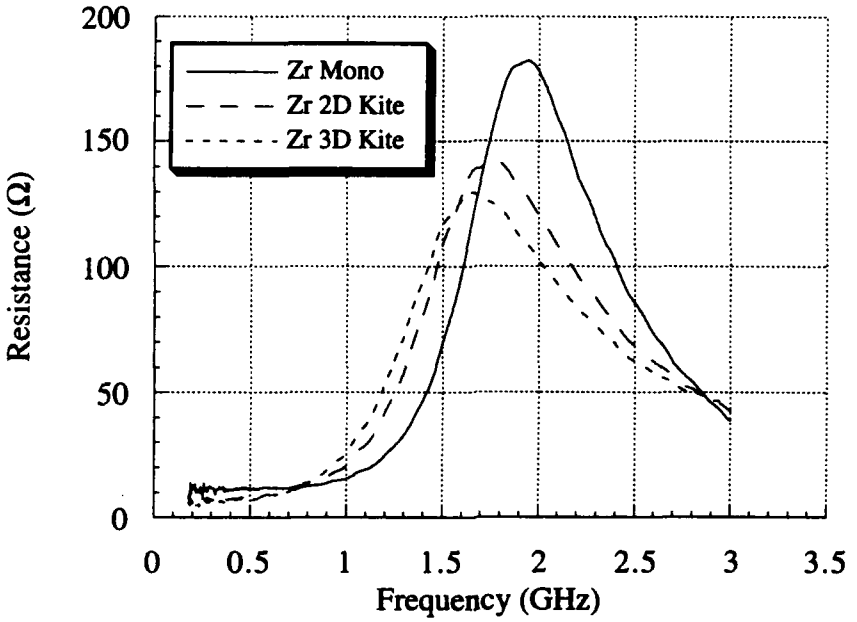

(a)

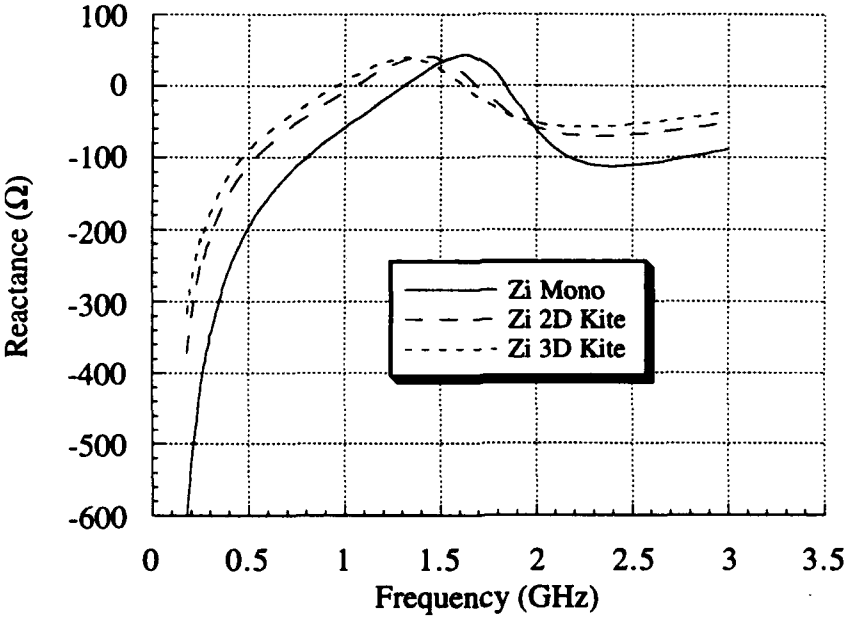

(b)

Figure 4.5 Impedance comparison of a linear monopole and kite geometries: (a) resistance (b) reactance.

the vertically polarized signal desired. Since a pattern null appears at the tip of a monopole, with this configuration there would be zero radiation in the direction of the line terminations along the horizon, which is unacceptable for mobile ground communications. Therefore, in another effort to increase the length of the conducting material without the efficiency and pattern deficiencies, the linear monopole was bent to an angle 20° above the horizon with a 1.67 cm stub at the feed. This geometry shown in Figure 4.6 was labeled the "gamma" antenna due to a slight resemblance to the Greek character, which increased monopole length by 229%. This changed the $\lambda/4$ resonant point from 1.47 GHz for the 5.1 cm linear model to 642.7 MHz for the 11.67 cm gamma. Bending the conductor allowed the increased length without sacrificing in the E_θ far-field. This model was appealing in that it had a simple form and was not likely to resist vehicle movement when mounted properly. The impedance characteristics are shown in Figures 4.7(a) and (b), which are also compared to the results for the modified NEC model. As expected, the increase in length helped the impedance at low frequencies; however, there were large variations after each resonant point. The design becomes better matched for higher frequencies though. This design was closely examined with different loading schemes.

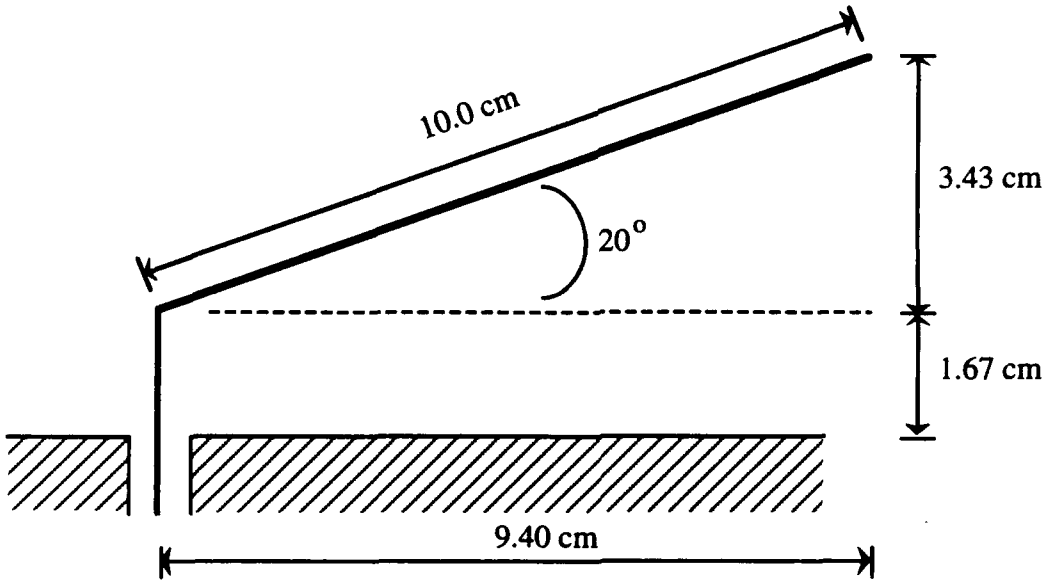

Figure 4.6 Gamma geometry.

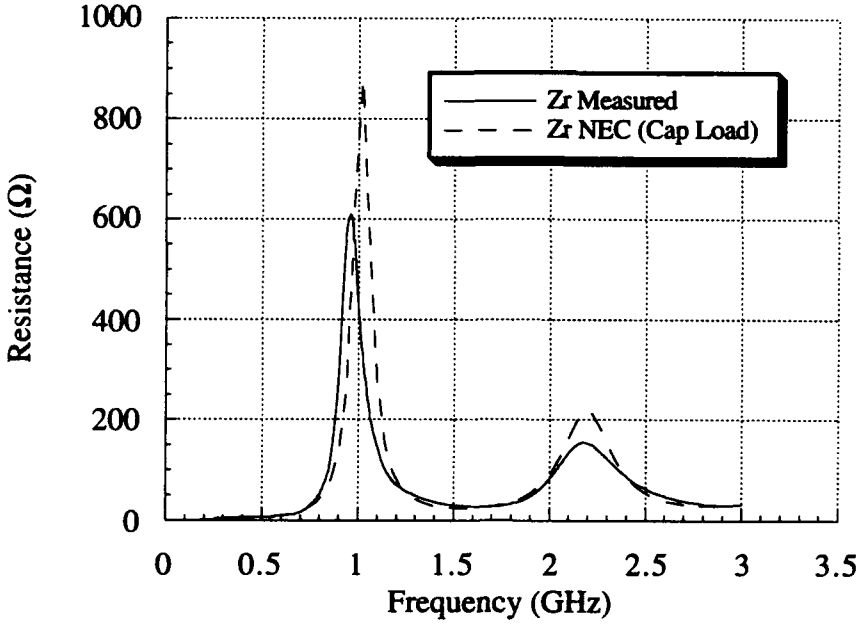

(a)

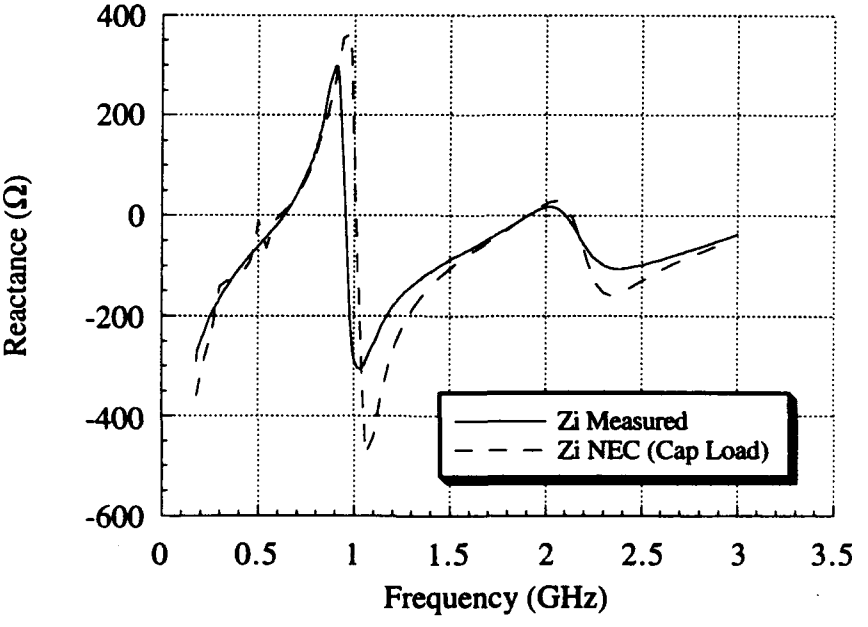

(b)

Figure 4.7 Gamma antenna impedance, measured and computed:
(a) resistance (b) reactance.

Despite the pleasing aesthetics of this design, the pattern was measured to be somewhat weighted towards the extended arm at higher frequencies. Figures 4.8(a)-(l) contain a series of radiation patterns for vertical polarization (E_θ) that spans the operating frequency range. On the left side of the page, the patterns show ϕ cuts (side views) where θ varies from 0^o to 90^o for both $\phi=0^o$ and 180^o. The right side of the page has θ cuts (top views) where $\theta=90^o$ and ϕ varies from 0 to 360^o. Patterns for a particular frequency are listed next to each other and are oriented according to an antenna bent to the left (along the positive x-axis). Not only is the energy directed to the left at higher frequencies, but the pattern fragmentation creates nulls that are unacceptable for a ground communication application. In addition, considerable radiation is lost at the higher elevations which further deteriorates the low-elevation power levels. In order to correct this problem, multiple gamma models were developed. It was thought that by creating a symmetric geometry the design would inherit a more omnidirectional pattern and better impedance values. These designs are described in the next section.

4.1.4 "Y" and "X" geometries

The multigamma approaches diagrammed in Figure 4.9 produced interesting results. The first of these geometries was formed by adding a mirror image of the gamma in the same plane as the original creating a two-arm antenna labeled the "Y." The second geometry repeated the gamma shape every 90^o forming a four-arm "X" antenna. The additions not only balanced the symmetry of the antenna for pattern purposes, but also increased the antenna volume while increasing conductor length. The effect of the larger antenna size can be seen in the impedance comparison plots in Figure 4.10. The larger the effective volume, the lower the impedance amplitudes as expected by previous results. In order to see the positive effects of the geometry on the radiation, an additional study was performed to compare with the results for the gamma. The far-field patterns are organized in Figures 4.11(a)-(l) where the Y antenna results are found on the left and the X antenna patterns are contained on the right. All plots represent cuts with θ fixed at 90^o. In each case, the antenna was situated with arms extending

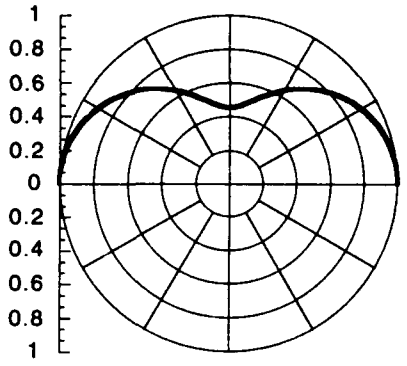

(a) Phi Cut @ 0.5 GHz

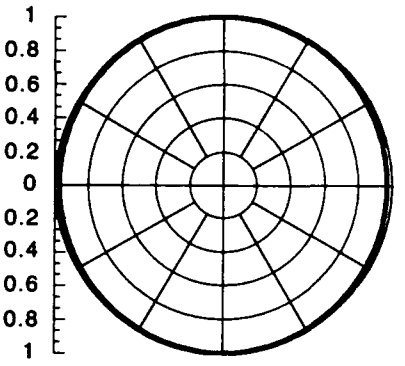

(b) Theta Cut @ 0.5 GHz

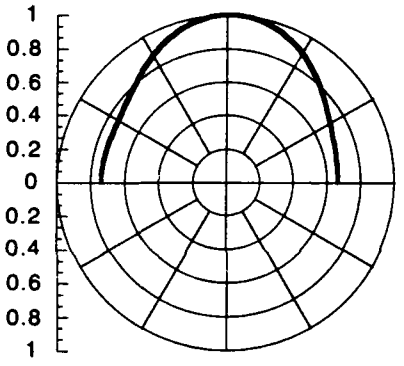

(c) Phi Cut @ 1.0 GHz

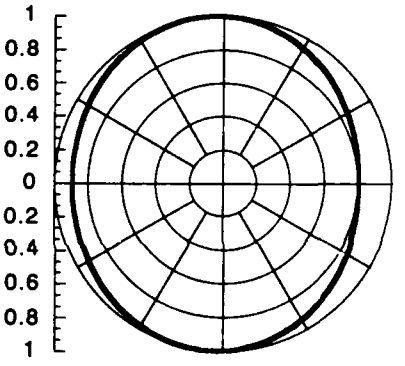

(d) Theta Cut @ 1.0 GHz

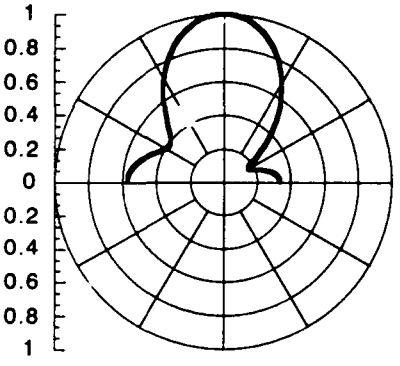

(e) Phi Cut @ 2.0 GHz

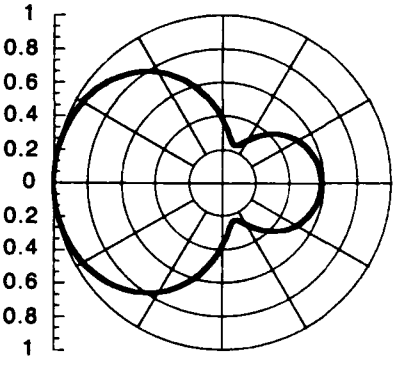

(f) Theta Cut @ 2.0 GHz

Figure 4.8 Normalized radiation patterns for a gamma antenna: structure is aligned along the horizontal axis with arm bent towards the left.

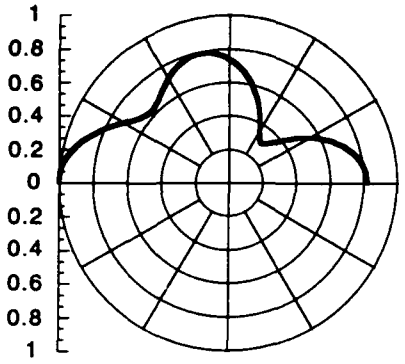

(g) Phi Cut @ 2.0 GHz

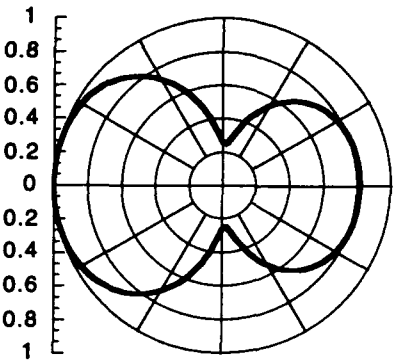

(h) Theta Cut @ 2.0 GHz

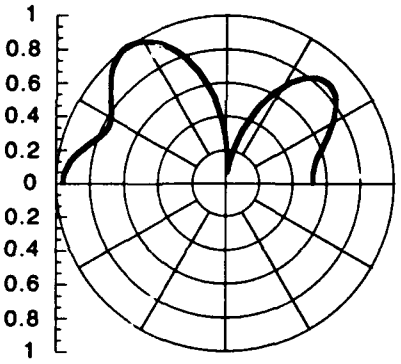

(i) Phi Cut @ 2.5 GHz

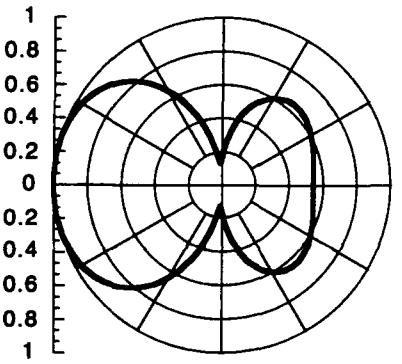

(j) Theta Cut @ 2.5 GHz

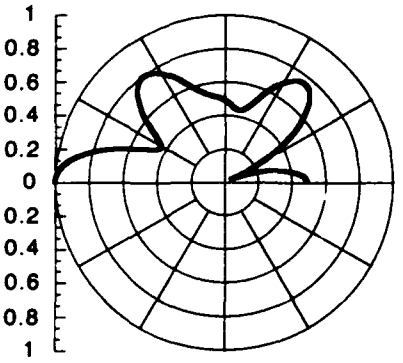

(k) Phi Cut @ 3.0 GHz

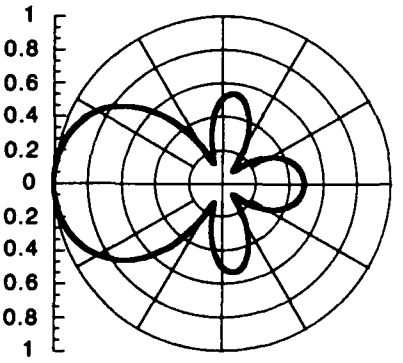

(l) Theta Cut @ 3.0 GHz

Figure 4.8(cont.) Normalized radiation patterns for a gamma antenna: structure is aligned along the horizontal axis with arm bent towards the left.

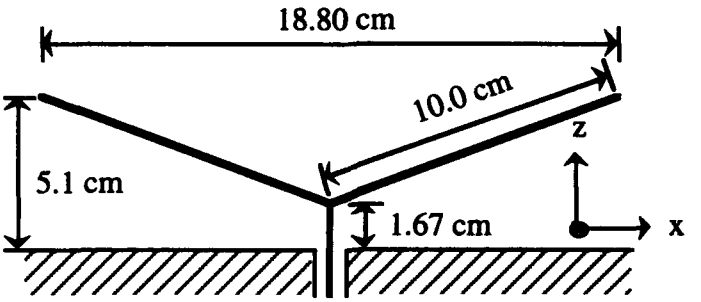

(a) "Y" Geometry

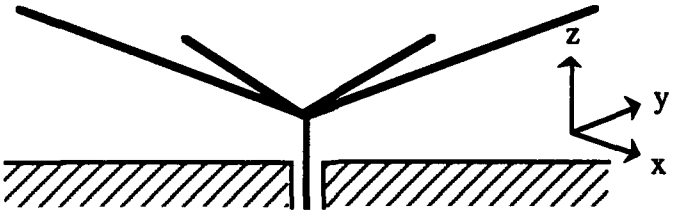

(b) "X" Geometry

Figure 4.9 Extended Gamma Geometries

along the horizontal axis (and vertical axis for the X geometry) of the figures. Although the Y antenna maintains a symmetric far-field pattern, radiation is not evenly distributed as ϕ varies. The X antenna develops a reasonable omnidirectional pattern throughout the frequency range. Despite the far-field improvements, these antennas were too unwieldy for a battlefield mobile communication system.

4.1.5 Antenna meandering

The concept of antenna meandering stems from the desire to increase conductor length within a confined space. The process of meandering requires a linear structure to be folded repeatedly to increase conductor length without a significant increase in antenna volume. Two meandered geometries were examined, and are pictured in Figures 4.12(a) and (b). The first merely wraps a linear monopole back towards the ground plane. The second meander takes place in the plane of the angled arm of the gamma geometry. The problem with these meandering geometries was that coupling occurred between adjacent conductors. Therefore, low-frequency improvements were overshadowed by the interaction of closely spaced antenna

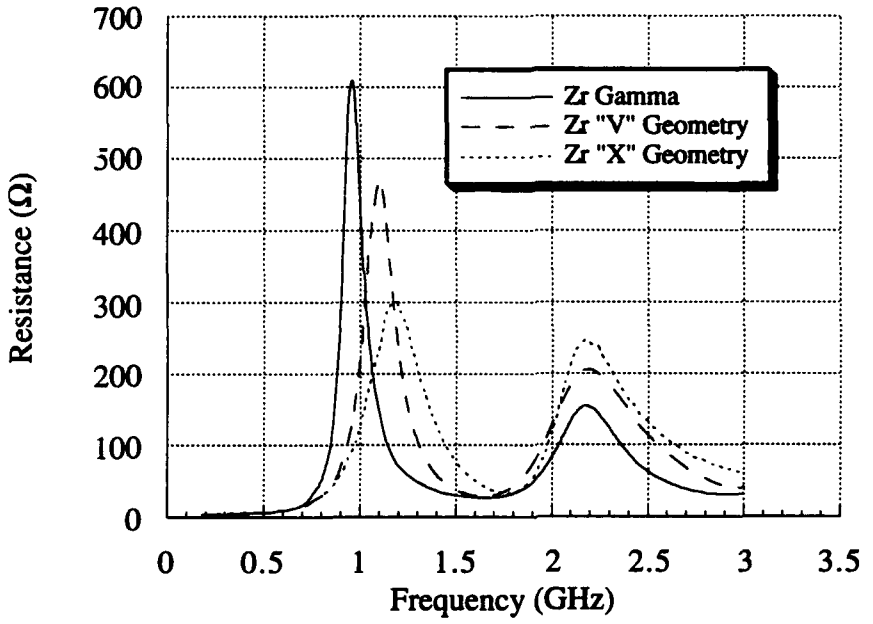

(a)

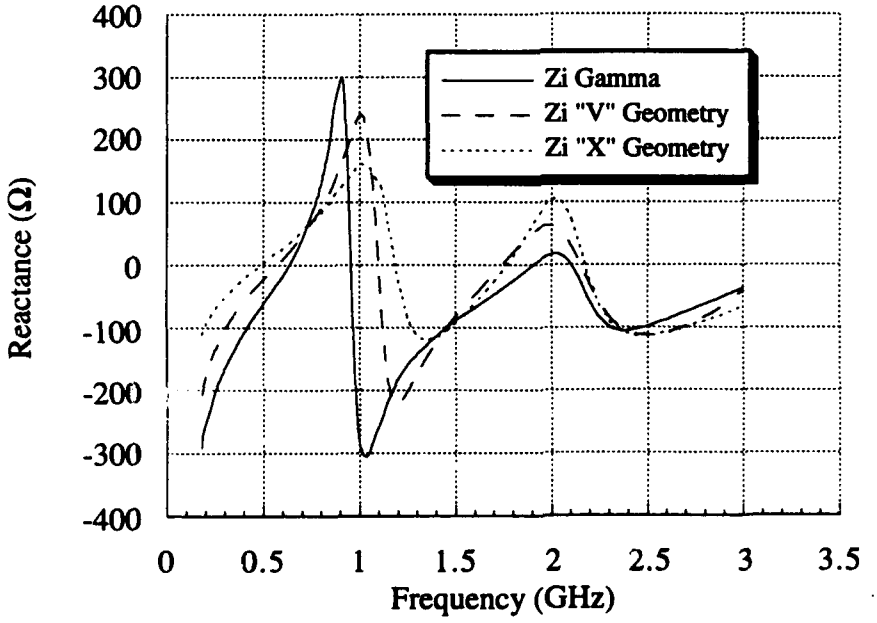

(b)

Figure 4.10 Measured impedance comparison between gamma, Y, and X geometries: (a) resistance (b) reactance.

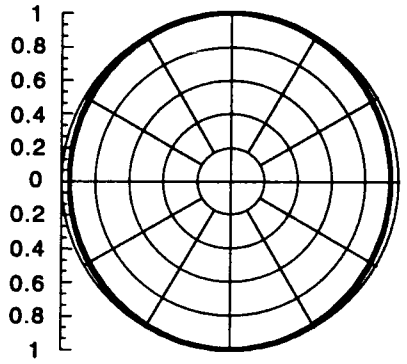

(a) Y @ 0.5 GHz

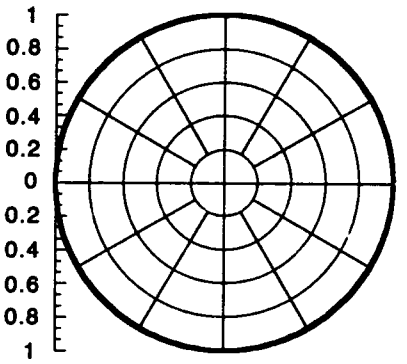

(b) X @ 0.5 GHz

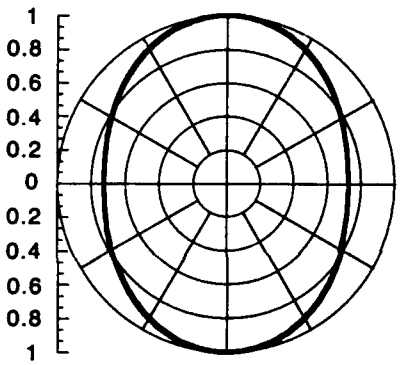

(c) Y @ 1.0 GHz

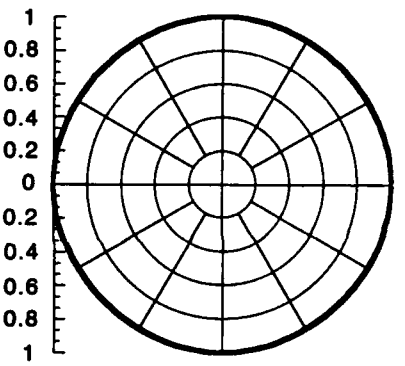

(d) X @ 1.0 GHz

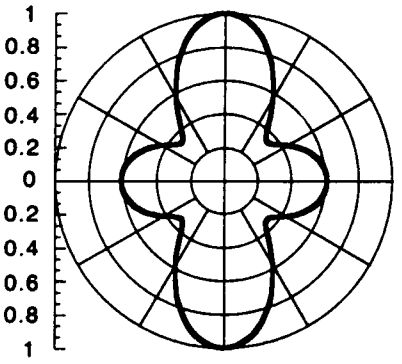

(e) Y @ 1.5 GHz

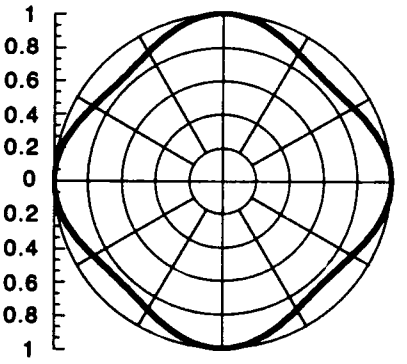

(f) X @ 1.5 GHz

Figure 4.11(a)-(f) Normalized radiation patterns for Y (left) and X (right) antennas: structure is aligned along the horizontal axis.

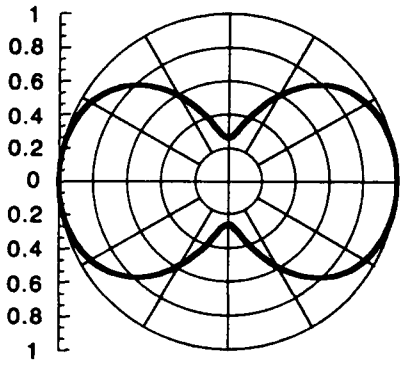

(g) Y @ 2.0 GHz

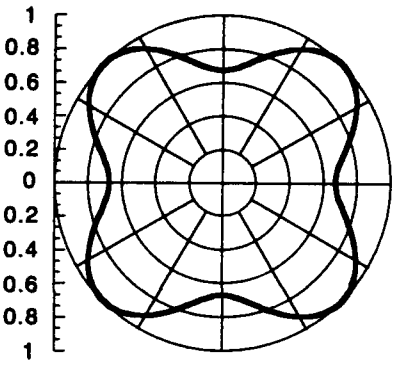

(h) X @ 2.0 GHz

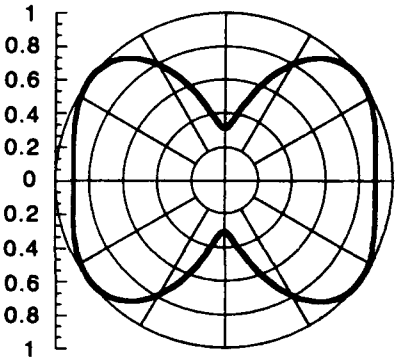

(i) Y @ 2.5 GHz

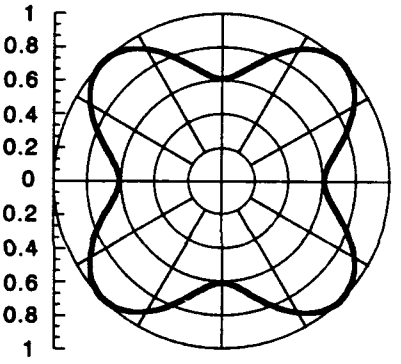

(j) X @ 2.5 GHz

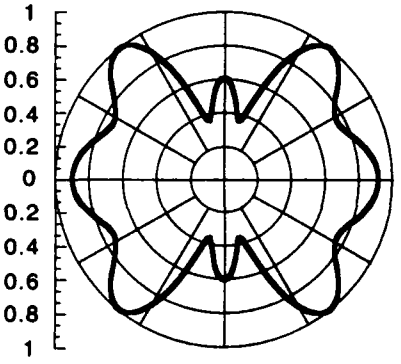

(k) Y @ 3.0 GHz

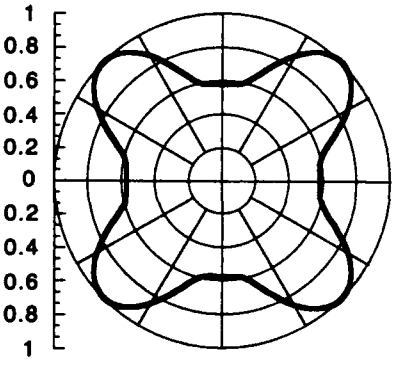

(l) X @ 3.0 GHz

Figure 4.11(g)-(l) Normalized radiation patterns for Y (left) and X (right) antennas: structure is aligned along the horizontal axis.

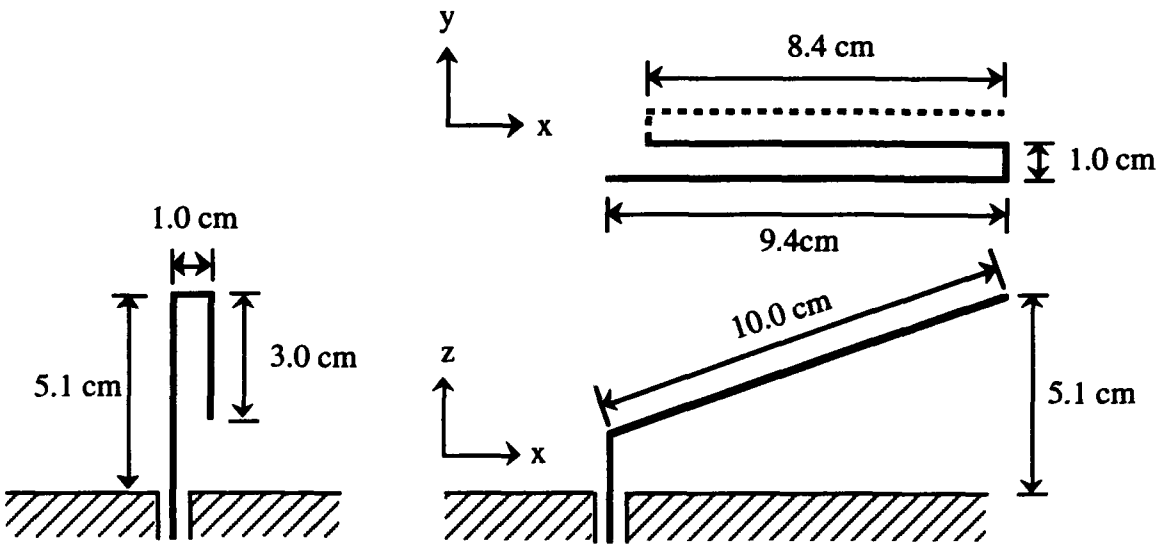

(a) linear meander (b) gamma meander

Figure 4.12 Meandering geometries

wires, which resulted in large variations in resistance and reactance for both models. Although the meander was not further examined, the geometry in 4.12(a) led to the development of the folded gamma antenna that was eventually chosen for the application.

4.2 Lumped Loading

Variation in geometry alone was not enough to develop a broadband antenna design for a low-profile, vehicle communication system. Therefore, emphasis switched to the application of lumped loading schemes to improve antenna performance. In Chapter 2, the high frequency response of lumped components was examined, and due to the great variation of the impedance of reactive components, research was limited to the analysis of resistive loading. It has been determined that by inserting a resistor a distance of $\lambda/4$ from the tip of a monopole, it can be terminated in its characteristic impedance which minimizes reflections from the end of the wire. More specifically, the addition that a 240 Ω resistance improves impedance characteristics by causing a large traveling wave to exist simultaneously with a small superimposed standing wave on the wire [9]. Using the lumped loading technique described in Chapter 2, various loading configurations were attempted with the geometric modifications discussed previously.

4.2.1 Resistive series-loading

The first loading configuration implemented Altshuler's technique [9]. The addition of a lumped resistive load in series with the antenna structure can improve the impedance characteristics. A diagram of the lumped loading system applied to the gamma geometry is shown in Figure 4.13.

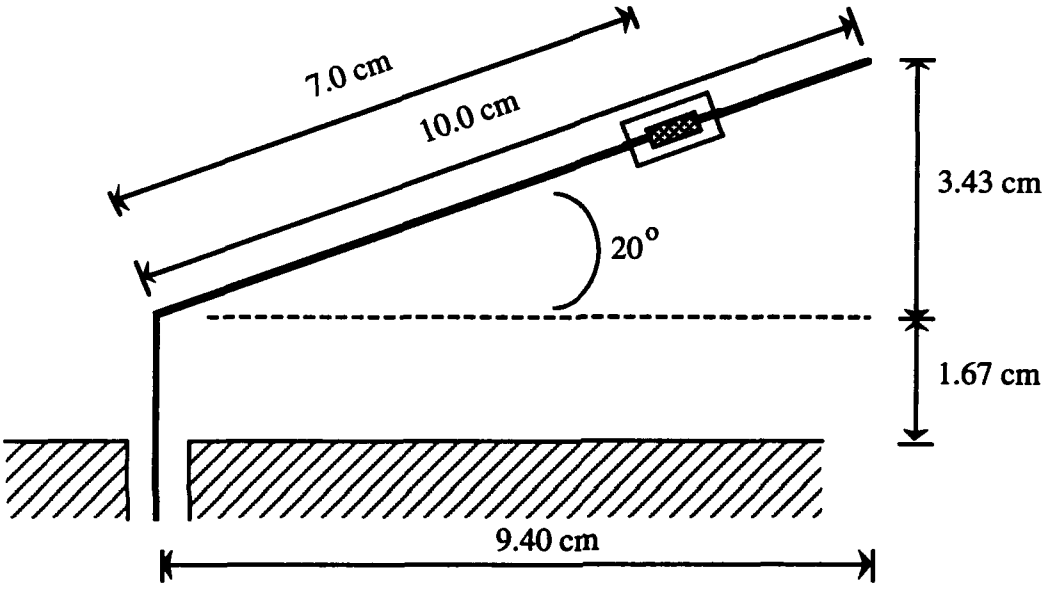

Figure 4.13 Lumped loading implementation.

For an impedance comparison, the load values were varied from 50 Ω to 240 Ω, and graphed in Figure 4.14. In each case, the impedance improved as the resistance increased, and the response was optimized with a 240 Ω resistor as expected from the literature [9]. Although the impedance amplitudes decreased, the low-frequency reactance was unaffected. In addition to this, the inclusion of the resistance decreased the efficiency of the radiated power since some was lost in the component. These losses, however, may be acceptable if the resulting impedance is made more easy to match to the generator system. Since the impedance match allows more energy to reach the antenna, this may account for the loss by the loading system. To solve the reflection problem for low frequencies though, it was necessary to implement a different resistive loading technique as described in Section 4.2.2.

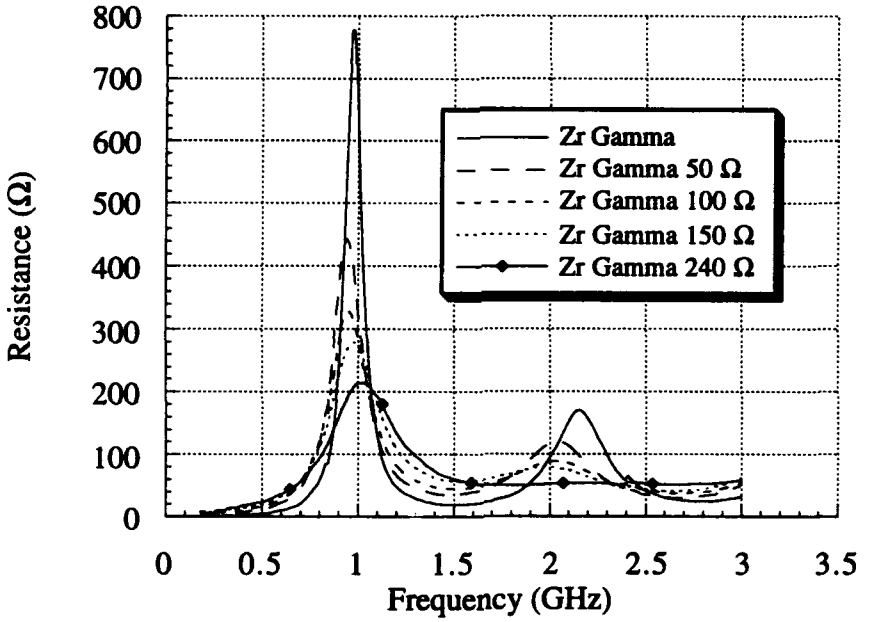

(a)

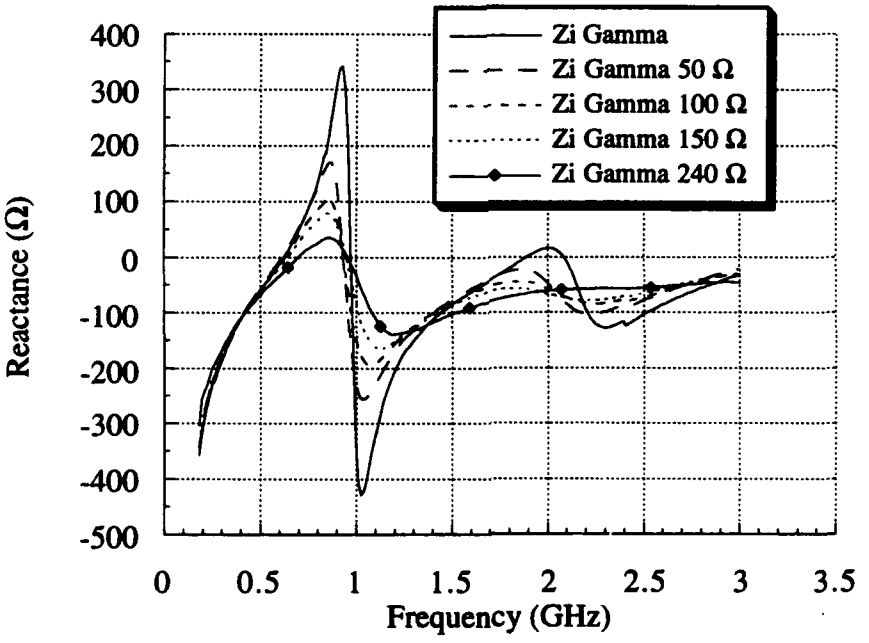

(b)

Figure 4.14 Measured impedance comparison for lumped loaded gamma geometry: (a) resistance (b) reactance.

4.2.2 Resistive tip-loading

Another lumped loading scheme analyzed in the laboratory consisted of connecting a resistive load from the monopole wire termination to the ground plane. In essence, this converted the gamma geometry into a loaded loop, which removed the problem of significant reflection especially at the lower frequencies. Tip-loading did not affect the higher frequency response where the impedance match was already acceptable. The loading technique is diagrammed in Figure 4.15 for the gamma antenna, and was easily adjusted for multiple gamma structures. In order to see the optimization of the 240 Ω resistance, each model was tested with a number of loading values. Figures 4.16-4.18 show the results for various load resistance values.

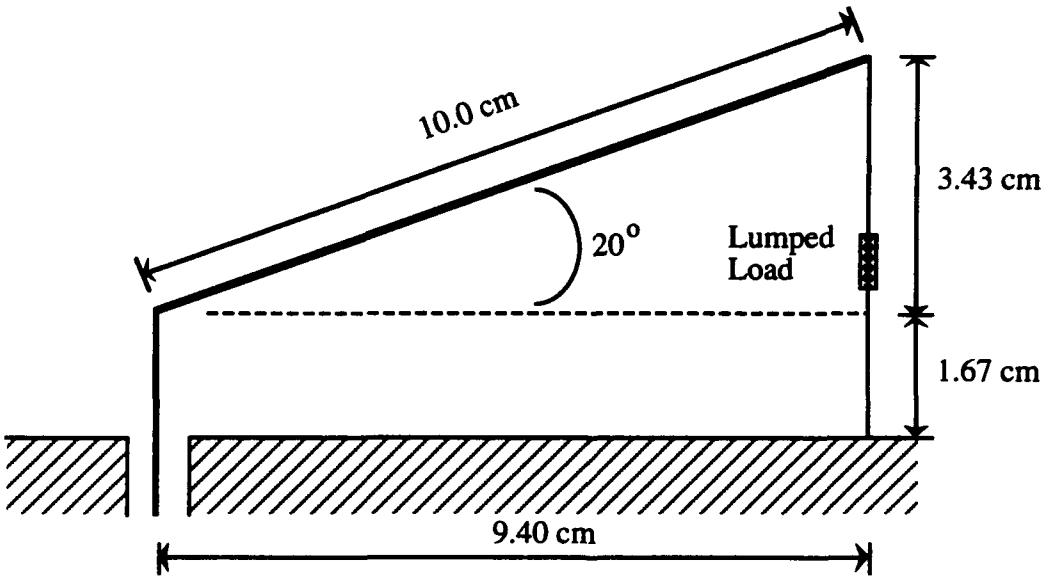

Figure 4.15 Resistively tip-loaded gamma antenna.

As expected, the impedance excursions were minimized with a load resistance of 240 Ω since the characteristic impedance was most closely matched just as in the other loading examples. Also, the increased conductor and antenna volume had the same positive effects as before. It should be noted that the advantage of these loading systems to the series resistances experimented with earlier focuses on the lowest points of the frequency range. Comparing the reactance characteristics of the series-loaded gamma with the tip-loaded gamma for 180 MHz,

the value has decreased from approximately -300 Ω to -80 Ω. This fact increases the matching potential of the second design over the first. Impedance matching will be discussed in Chapter 5. Because the Y and X geometries were too complex and space intensive, work progressed on simpler improvements of the 240 Ω tip-loaded gamma.

For a closer look at the impedance of this design, refer to Figure 4.19. Notice that despite the error in the resistor-only simulation in Chapter 2, when implemented on the antenna structure, the model follows measured data well. This demonstrates the utility of the parasitic capacitance modification and detailed geometric computer modeling for accurate simulation of antenna characteristics. Emphasis then changed to methods of antenna construction and the appearance of the far-field pattern.

In terms of mechanical realization, the tip-loaded gamma antenna presented some difficulties. First, the structure had two contact points with the ground plane which increased the surface area necessary for mounting. Secondly, the bend required reinforcement due to the size of the operational system and desire for a flexible arm. Next, the load resistor would have to be shielded. One method for accomplishing this included placing a grounded sheath over the loaded wire, a second method called for tubular antenna structure to allow the load to be placed within the conductor with a path to ground at the feed location. The experimental results of these investigations showed significant impedance degradation; therefore, these methods were not used.

The radiation of the unloaded gamma antenna was heavily weighted towards the direction of the extended arm; with the resistive load included, the pattern results were further degraded. Since the extended gamma geometries were discounted due to space considerations, smaller structural changes were attempted. The meandering linear monopole from Figure 4.12(a) was equipped with a tip-loaded resistor. This antenna required minimum volume and showed excellent omnidirectional characteristics; however, the efficiency of the small structure was found to be too low for the limited power supplies used in mobile communications. Numerical experiments were performed to do determine the effect of increasing the space be-

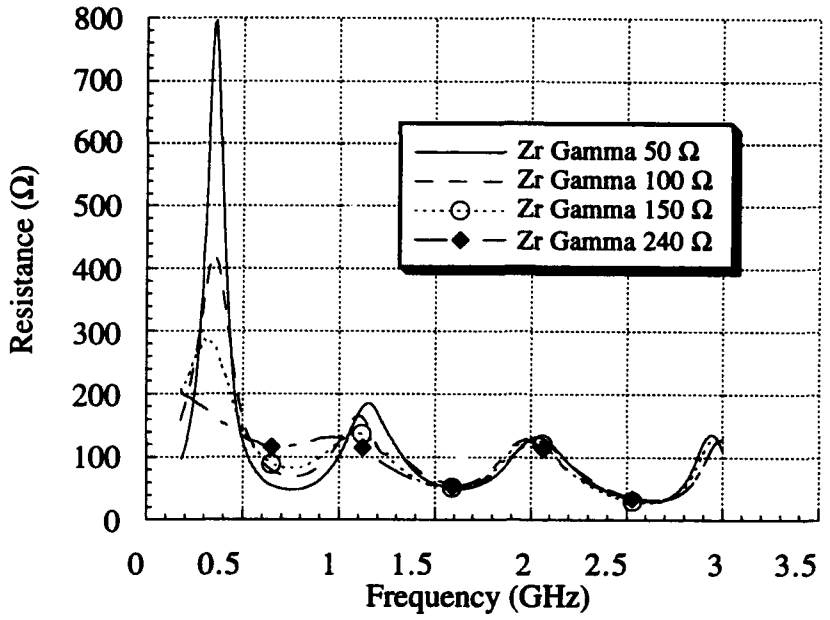

(a)

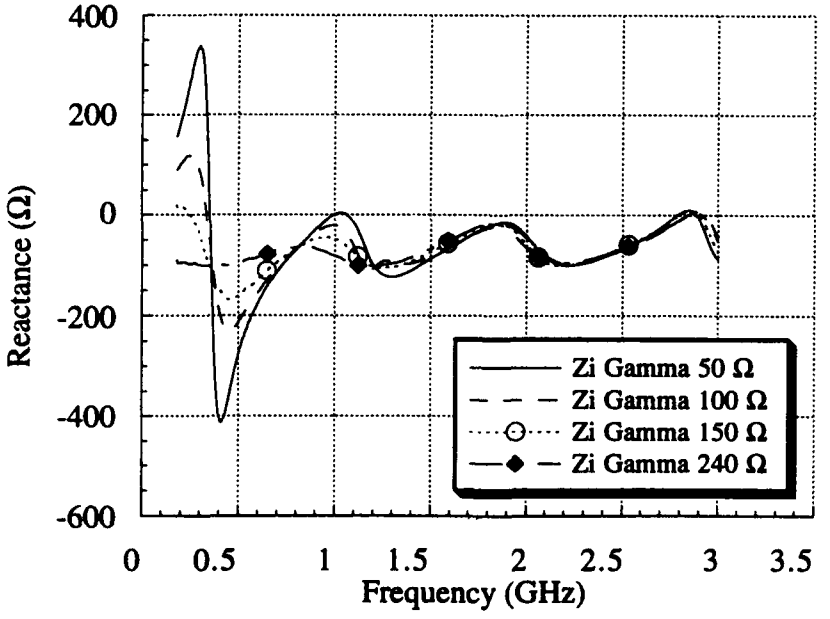

(b)

Figure 4.16 Measured impedance comparison for a tip-loaded gamma: (a) resistance (b) reactance.

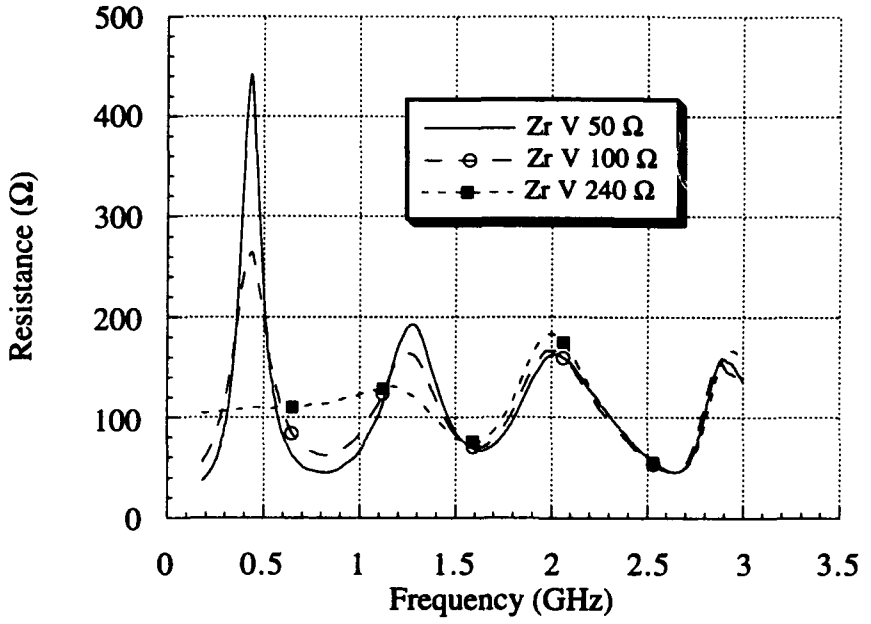

(a)

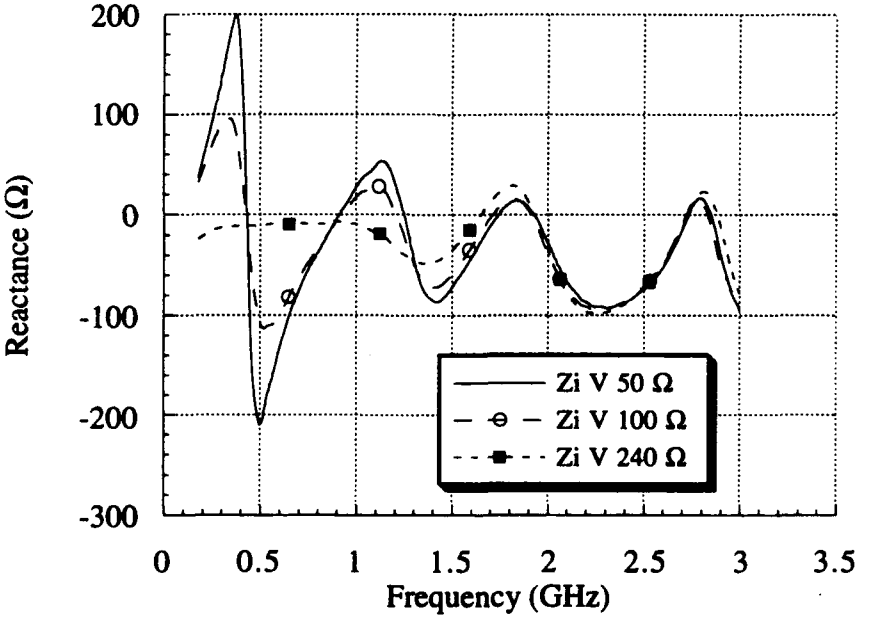

(b)

Figure 4.17 Measured impedance comparison for a tip-loaded Y: (a) resistance (b) reactance.

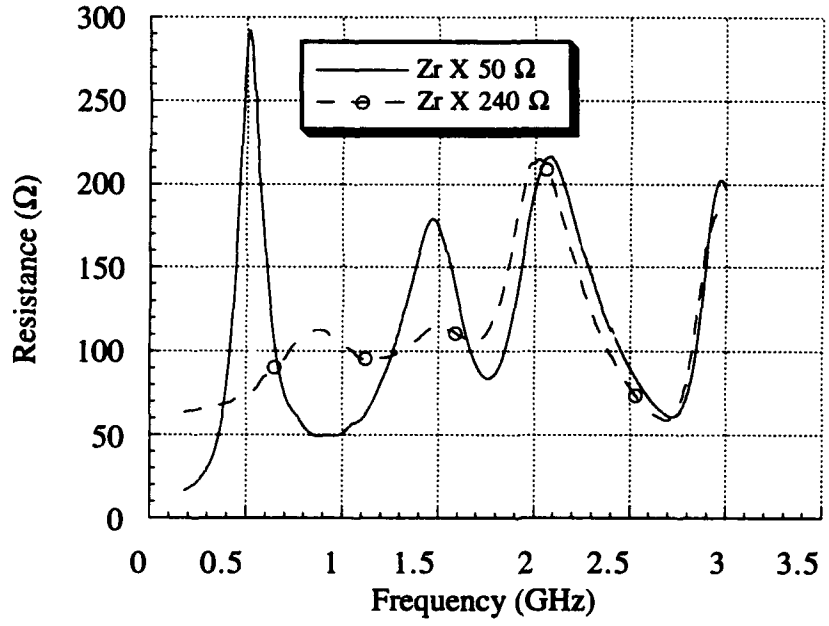

(a)

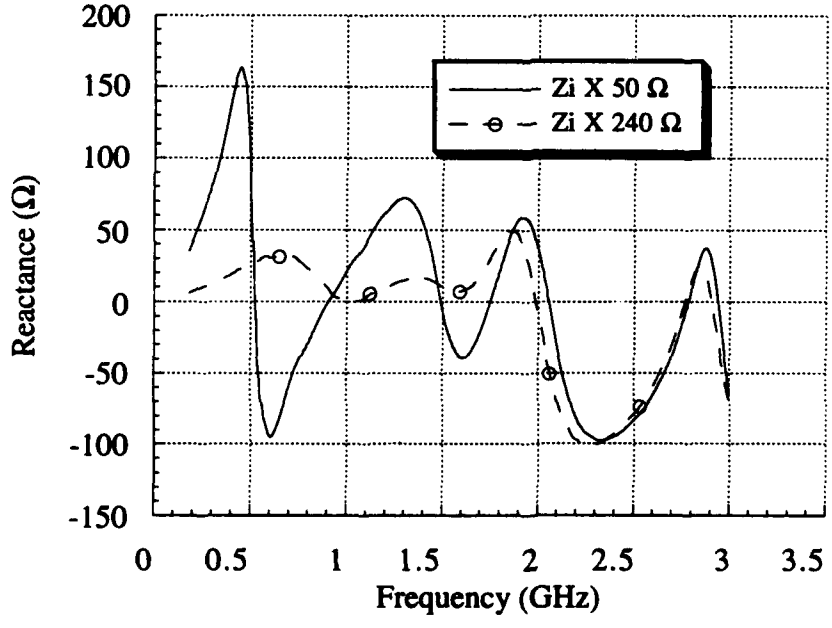

(b)

Figure 4.18 Measured impedance comparison for a tip-loaded X: (a) resistance (b) reactance.

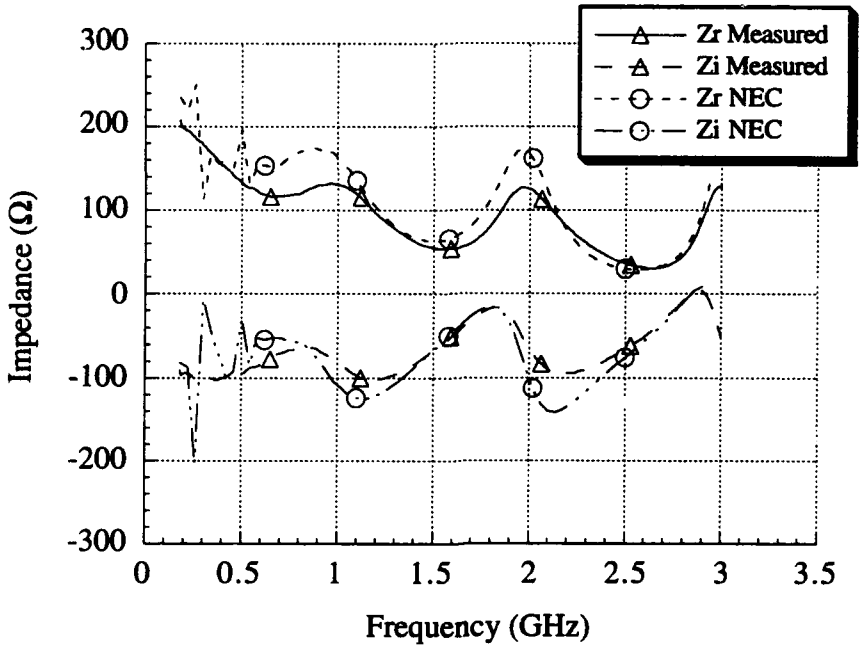

Figure 4.19 Measured impedance of a 240 Ω tip-loaded gamma antenna and corresponding NEC analysis: (a) resistance (b) reactance.

tween conducting wires to minimize coupling. It was determined that by extending the arm farther away from the feed, the impedance amplitude decreased. To maximize the effects of the current distribution on the antenna and create a strong E_θ pattern, it was desired to have a vertical conductor at locations where feed current would be the highest. The conductor separation distance was kept large to minimize coupling. At the same time, by forcing the feed and monopole termination to be in close proximity, the mounting area could be minimized. By folding the monopole into a triangular configuration, it was possible to develop a self-supporting structure with promising performance values. This geometry led to the folded gamma antenna which became the operational design. Figure 4.20 shows the progression of the folded gamma design. The third antenna includes a curved corner to make the structure less likely to be hung up on obstacles. This geometric modification did not seriously affect either the impedance or the pattern characteristics of the antenna.

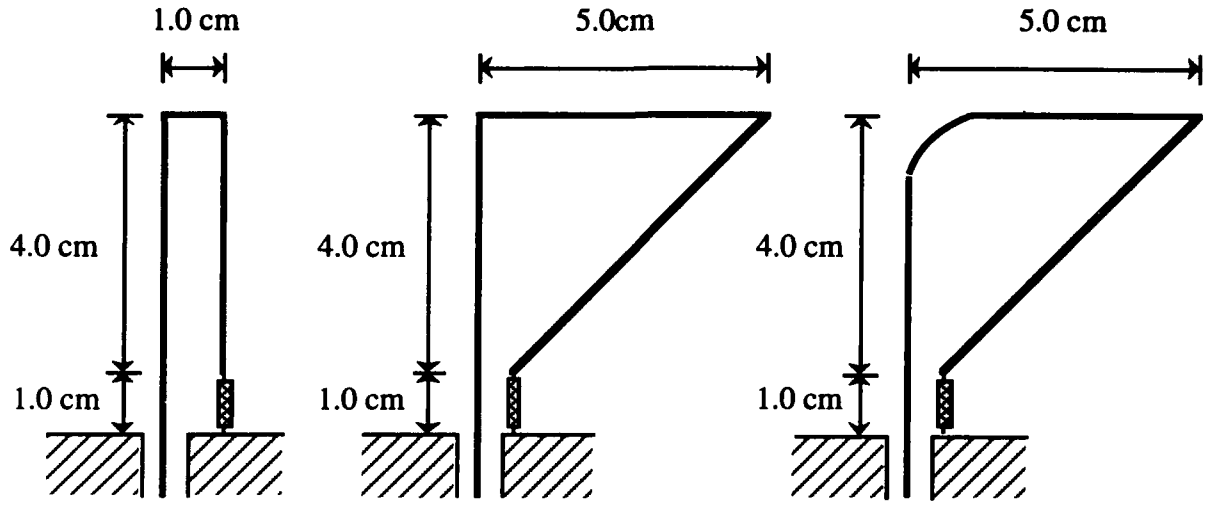

Figure 4.20 Progression of the folded gamma geometry.

The measured impedance of this design is compared to those for the tip-loaded gamma model in Figure 4.21. Figures 4.22(a)-(f) show a series of far-field θ cut patterns for both the tip-loaded gamma and folded gamma designs. These patterns are normalized to the maximum value of both antennas in order to have a radiation comparison for each frequency. The solid lines represent the tip-loaded gamma results while the dashed curves show the folded gamma far-field patterns. Notice that throughout the frequency range, the folded gamma maintained a relatively omnidirectional pattern. On the other hand, the tip-loaded gamma antenna radiation was dominant to the right (away from the lumped load) for low frequencies, but the pattern flipped to the left and fragments as frequency increased. Therefore, the folded gamma appears to be well suited to a mobile ground communication system.

4.3 Grounded Sleeves

Aside from the geometric alterations earlier conducted on the antenna, experimentation was also accomplished with the use of grounded sleeves for impedance improvement. As described in Chapter 2, sleeve structures were more easily constructed and measured in the laboratory than modeled on a computer. The sleeve model was realized by placing a conducting cylinder concentrically over the test monopole and attaching it to the ground plane. Sleeve length was varied in the laboratory based on fraction of the center monopole length.

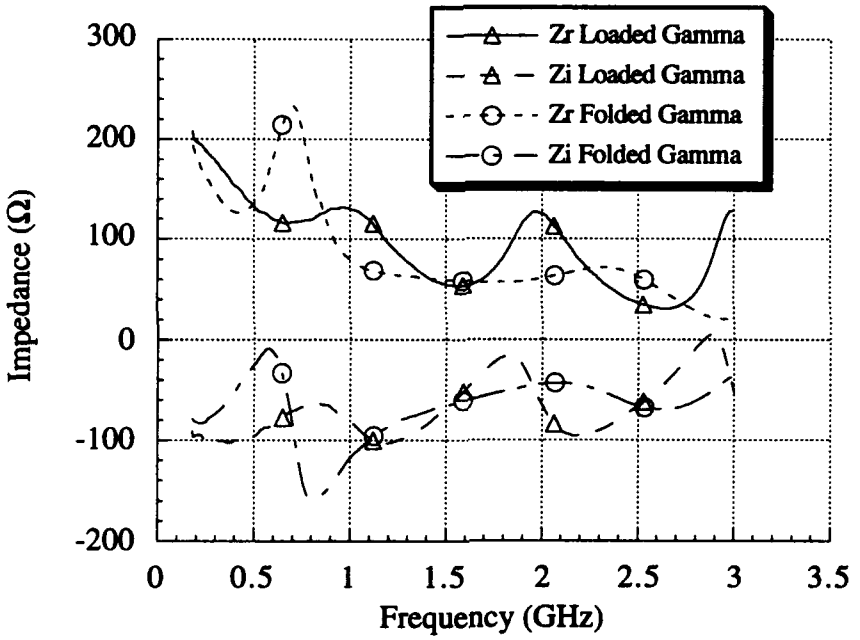

Figure 4.21 Measured impedances of a 240 Ω tip-loaded gamma and a folded gamma.

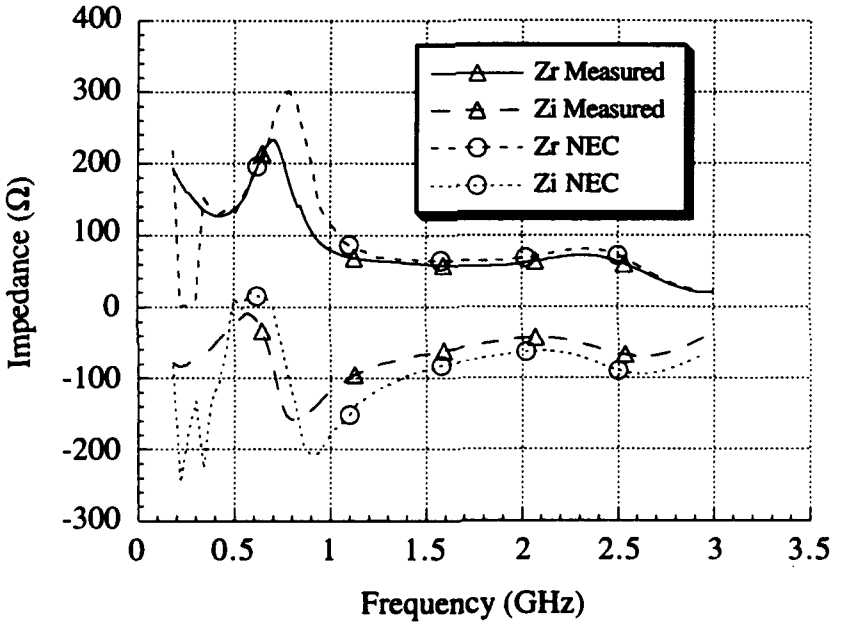

Figure 4.21 Measured impedance vs. NEC analysis for a folded gamma.

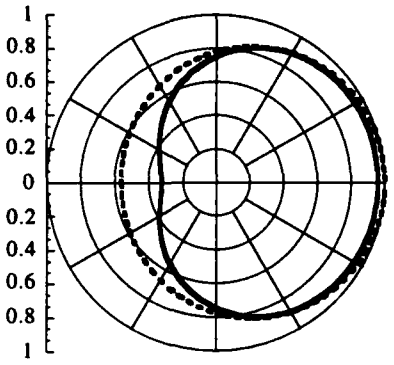

(a) 0.6 GHz

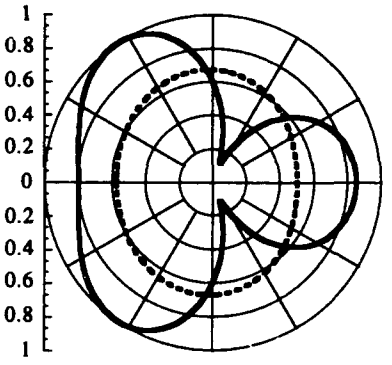

(b) 1.0 GHz

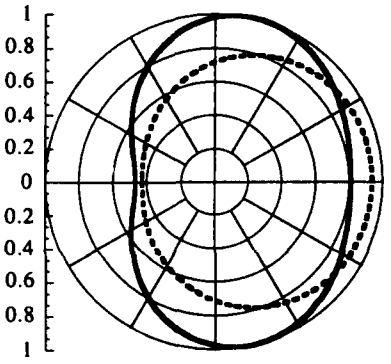

(c) 1.4 GHz

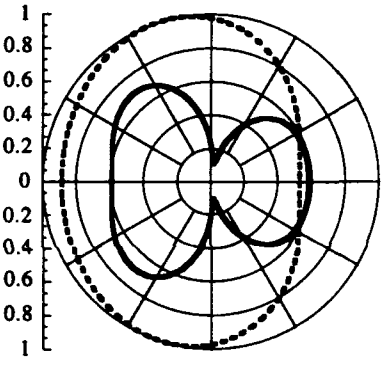

(d) 1.8 GHz

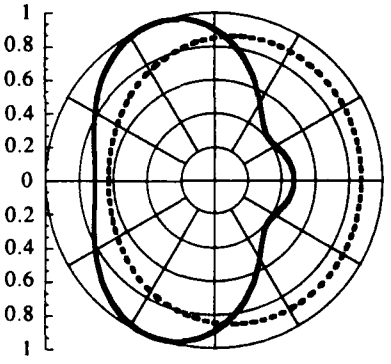

(e) 2.2 GHz

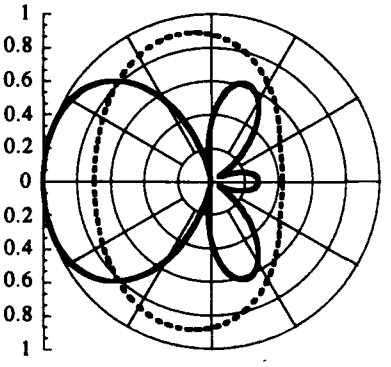

(f) 2.6 GHz

Figure 4.22(a)-(f) Radiation pattern θ cuts for a loaded gamma (solid line) and a folded gamma (dashed line).

The measured results for varying sleeve length appear in Figures 4.23(a) and (b). The addition of the sleeve helped the low-frequency characteristics, but as sleeve height increased, the performance at high frequencies decreased. Therefore, the grounded sleeve seems to be useful for impedance improvement across a certain band of frequencies, and its height will determine which range is applicable.

In another experiment, short sleeves were excited to realize a two-antenna system for low and high frequencies with omnidirectional radiation patterns. It was thought that sleeves of varying heights could be positioned concentrically to create a multiband antenna system. The physical models failed to develop a horizontally dominant radiation pattern due to coupling with structures inside the sleeve. The array analyses in Section 4.4 provided the explanation for this. The scalloped radiation pattern was due to the small sleeve radius. For more information about grounded sleeves and excited sleeves see the literature [4].

4.4 Arrays

The final concept for broadbanding that was experimentally analyzed dealt with the combination multiple antennas in arrays for multiple band transmission. The design originated with the examination of two linear antennas placed next to each other, a long monopole for low frequencies and a shorter version for a higher band. Radiation patterns measured in the laboratory showed that although the large monopole was negligibly affected by the presence of the smaller one, the inverse was not true. The smaller antenna could not seem to radiate *through* the low frequency monopole due to coupling. A simple solution to this called for the addition of a duplicate antenna on the opposite side of the large radiator to balance out the pattern. This operation succeeded, and experimentation of this configuration led to the determination of a subtle relationship between adjacent radiators. Since the amount of coupling between two antennas is indirectly proportional to the distance between them, increasing the separation distance causes less performance degradation. With the third antenna included, however, the analysis became much more complicated. Figure 4.24 details the geometry of the

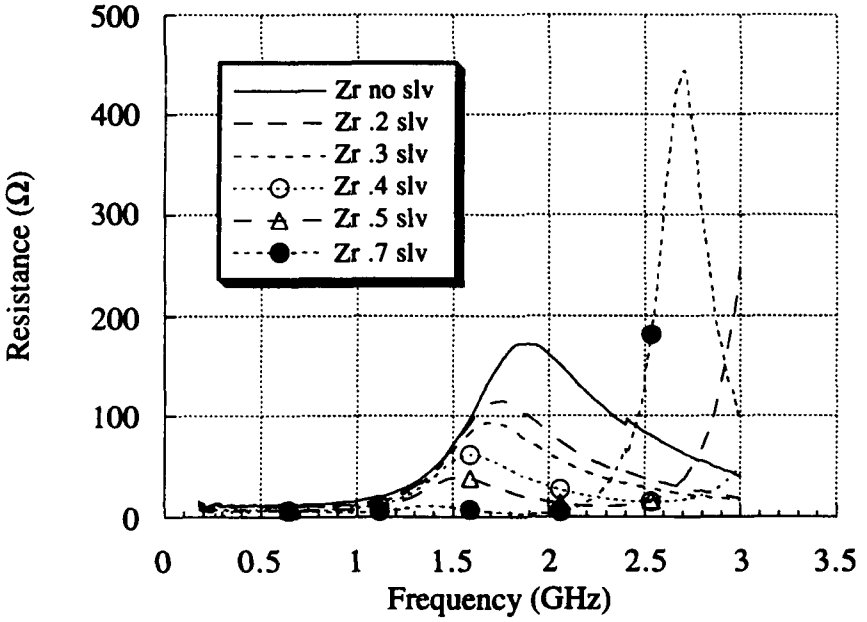

(a)

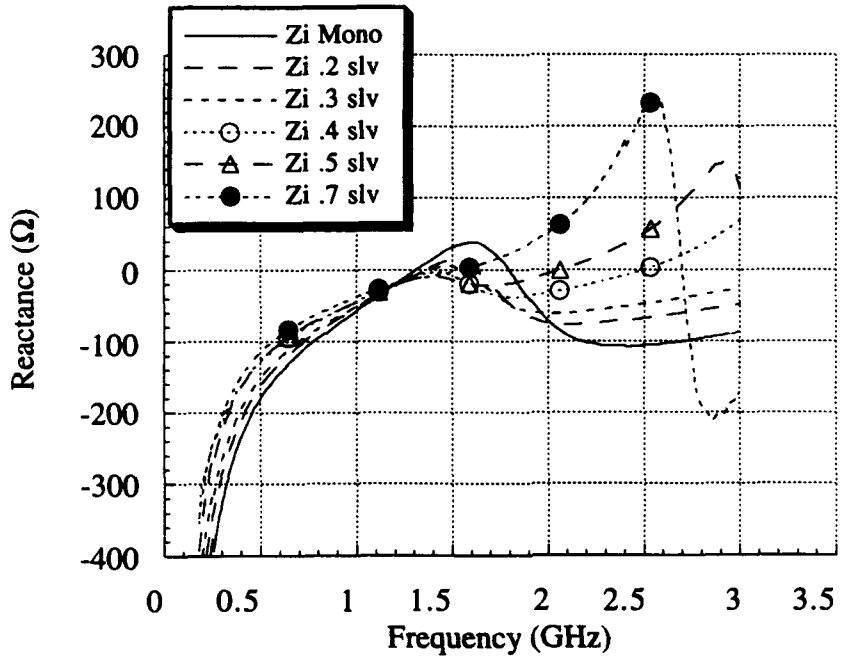

(b)

Figure 4.23 Measured impedance of variable height grounded sleeves: (a) resistance (b) reactance.

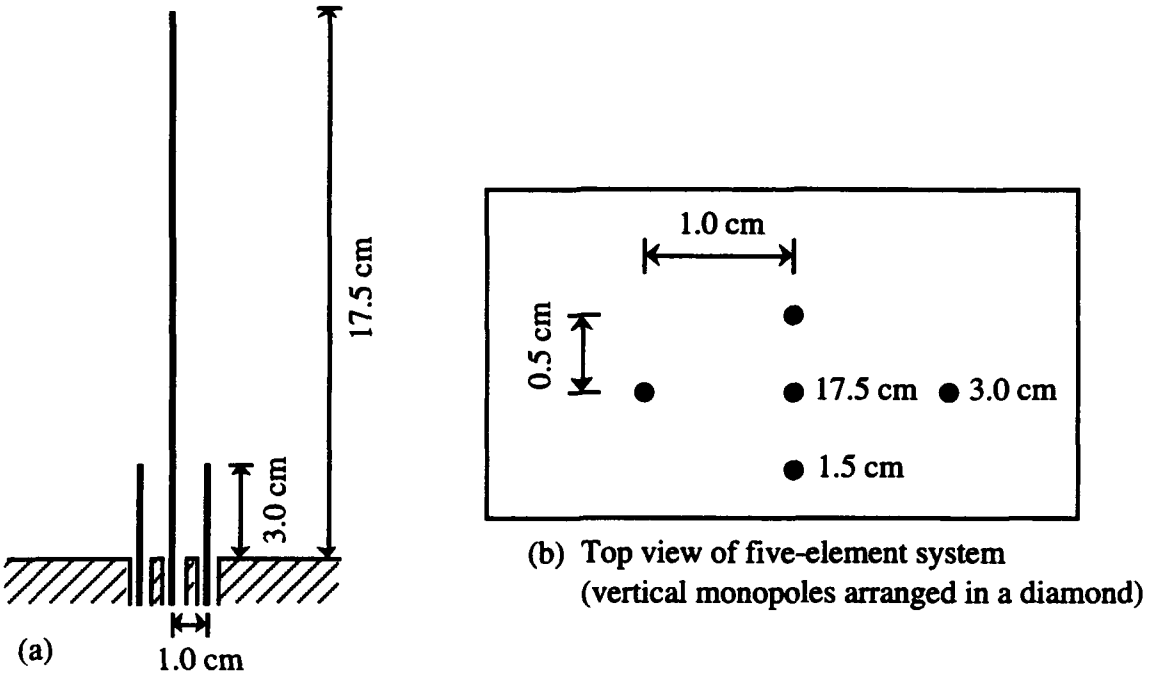

Figure 4.24 Array Systems (a) three-antenna system
(b) placement of five-antenna system.

three-antenna system. The center conductor measured 17.5 cm and operated at low frequencies since it resonated around 428 MHz. The smaller monopole had a 3.0 cm height which corresponded to a 2.5 GHz resonance. For arbitrary applications, these heights can be determined by the engineer for particular frequency bands.

Therefore in order to develop a system, after choosing monopole lengths, the only parameter to set is the separation distance. Coupling of the large antenna resulted in large amounts of power to be radiated at higher elevations. Because this was not acceptable for a ground communication application, the separation distance was increased to minimize these effects. Since the coupling is inversely proportional to the distance, it would appear that a large separation would be optimum. However, the problem presented with a large distance between elements deals with the θ cut pattern lobe generation as described in the literature [10]. As the array elements move apart, the omnidirectionality of the pattern decreases. Therefore, the array combination had to be designed such that minimal coupling occurred with maximum omnidirectionality, a trade-off between wide and narrow separations. As elements become

shorter for higher frequency, the separation distance must decrease accordingly. Once an acceptable design in two dimensions was complete, a third set of monopoles was added to operate at even higher frequencies with 1.5 cm height in order to resonate at approximately 5 GHz (see Figure 4.24(b)).

The question then arose about how to terminate nonexcited elements while radiating on a certain channel. A graph of the segment currents with the midband monopoles excited is shown in Figure 4.25 . The other antennas were terminated with an open, short, and matching load to determine the minimum coupling current configuration. From this we determined that the nonradiating monopoles should be shorted to ground during operation. Following the current analysis, the radiation patterns for the antenna systems are presented in Figures 4.26-4.27. For the most part, the power remains close to the horizon with a reasonably omnidirectional distribution.

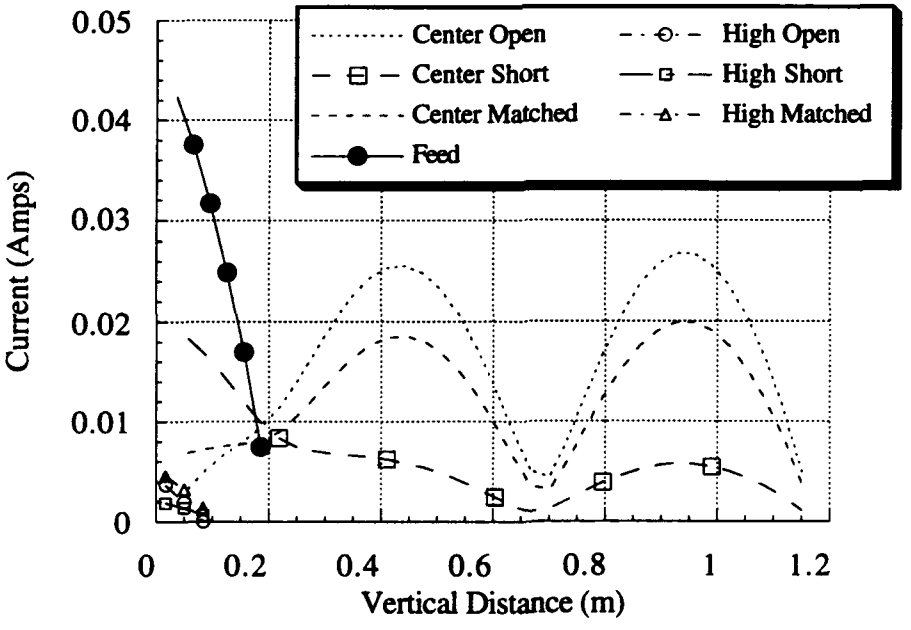

Figure 4.25 Segment currents on five-antenna system: midrange monopoles excited.

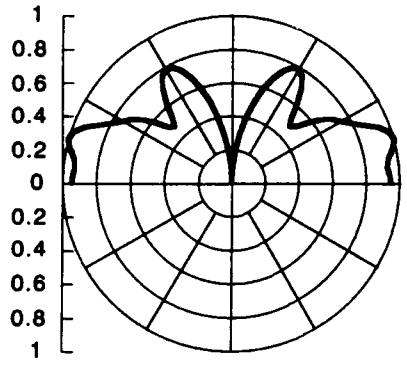

(a) Array Phi Cut @ 3.0 GHz

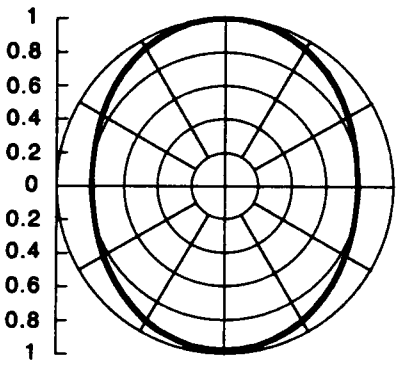

(b) Array Theta Cut @ 3.0 GHz

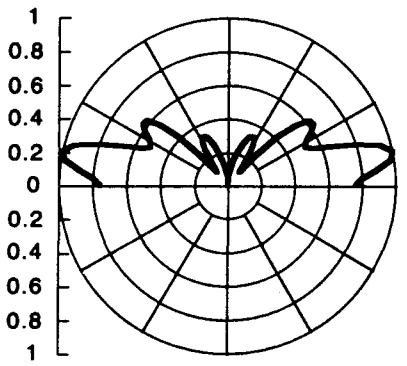

(c) Array Phi Cut @ 4.0 GHz

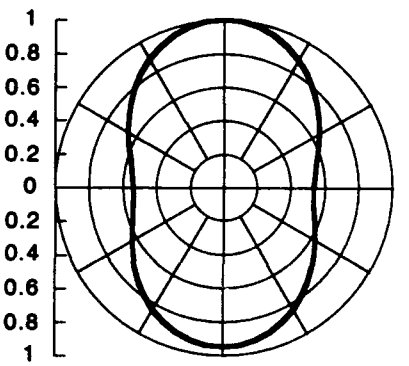

(d) Array Theta Cut @ 4.0 GHz

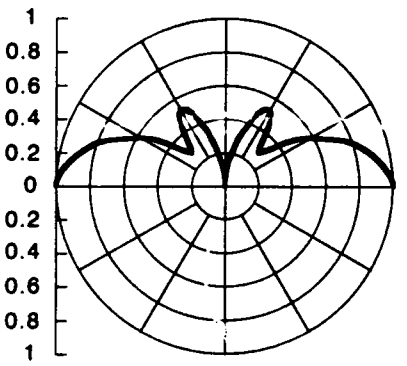

(e) Array Phi Cut @ 5.0 GHz

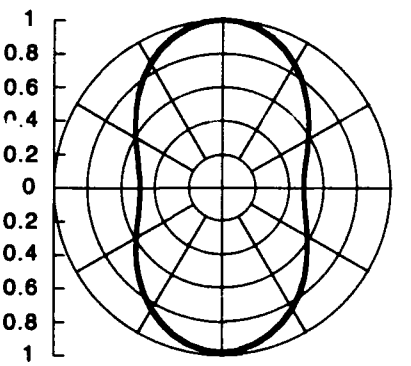

(f) Array Theta Cut @ 5.0 GHz

Figure 4.26 Radiation patterns for five-element antenna system: midrange monopoles excited, others shorted.

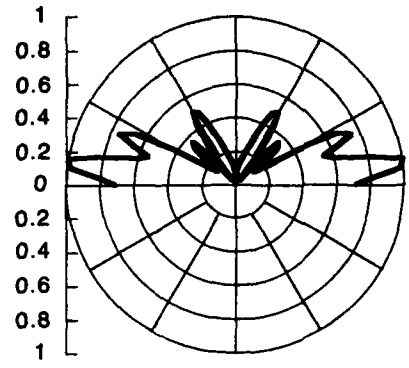

(a) Array Phi Cut @ 6.0 GHz

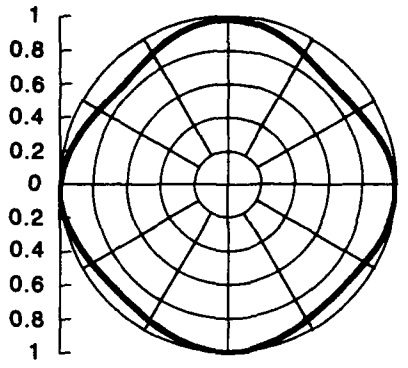

(b) Array Theta Cut @ 6.0 GHz

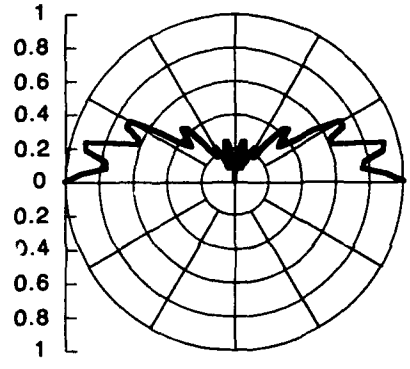

(c) Array Phi Cut @ 7.0 GHz

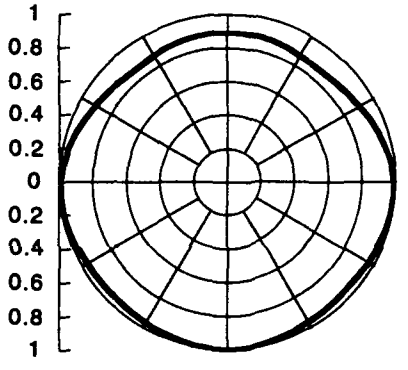

(d) Array Theta Cut @ 7.0 GHz

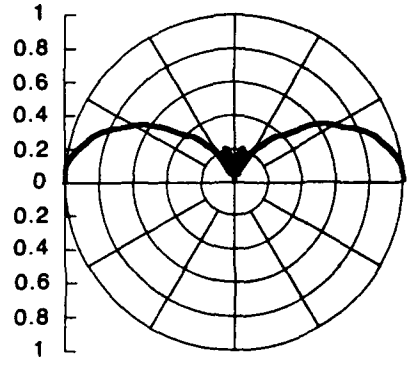

(e) Array Phi Cut @ 8.0 GHz

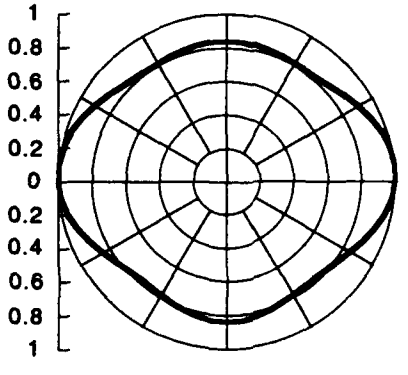

(f) Array Theta Cut @ 8.0 GHz

Figure 4.27 Radiation patterns for five-element antenna system: high-range monopoles excited, others shorted.

4.5 Broadbanding conclusions

In this chapter, various methods of broadbanding were examined. Each of the methods was measured in the laboratory, most of which were also analyzed using NEC. From the systematic refinement of geometry and loading, a folded gamma antenna was developed that meets the design specifications for a low-profile, broadband, monopole vehicle antenna for use in mobile ground communication. In addition to this, the use of grounded sleeves and array combinations was viewed for their application to the broadbanding process.

5. MATCHING NETWORK GENERATION

The ability of an antenna to radiate optimally depends on numerous factors. One very important radiation parameter deals with the impedance mismatch between the antenna and its source. Using a transmission line analogy from basic electromagnetics, changes or discontinuities in impedance cause signal reflections as a wave propagates down a line. The reflections lead to interference which decreases the quantity of the signal that is actually transmitted over the line. The same is true in an antenna system; regardless of the device design, these achievements could be useless if the antenna is not properly matched to its source. Therefore, the problem is to develop a lossless network that makes the impedance "seen" by the generator equal to that of the generator itself. By equating these two impedances, the power delivered to the antenna for radiation is maximized.

5.1 The Real Frequency Method

The Real Frequency Method (RFM) developed by Carlin [11] seeks to determine the circuitry necessary to maximize the power transfer from a generator to an arbitrary antenna. The key advantages of the RFM over those for previous matching networks theories are that there are no assumed models or analytic expressions necessary for the load. In addition, no assumptions are made for the form of the system transfer function. Figure 5.1 shows a block diagram of the matching network system. In the figure, Z_L represents the impedance of the antenna and Z_q is the matching network impedance that maximizes the power delivered to the

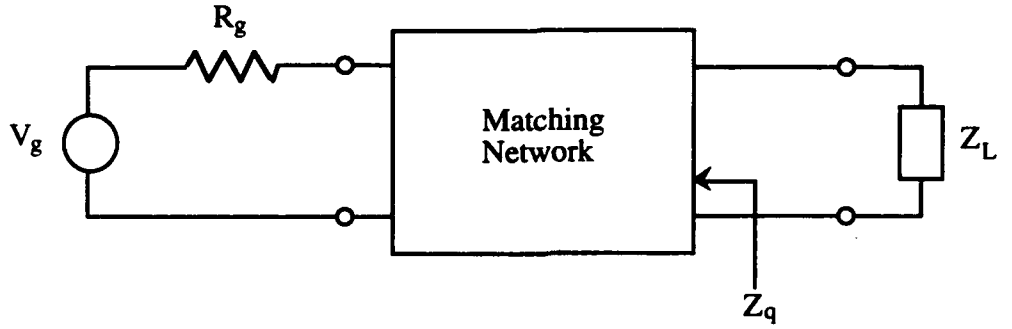

Figure 5.1 Diagram of matching problem.

load. To quantify the power interaction between the generator and the load, the Transducer Power Gain (TPG) is used. The TPG is defined as the ratio of the power delivered to the load to the power available from the generator. More specifically, it is given by

$$T(\omega^2) = \frac{\text{Power to Load}}{\text{Power Available from Generator}} = \frac{P_{in}}{P_{av}} = \frac{4R_q(\omega)R_L(\omega)}{\left|Z_q(\omega)+Z_L(\omega)\right|^2} \tag{5.1}$$

This is not a trivial problem because the impedance is a frequency-dependent complex value. However, there is a Cauchy-Riemann relation between the real and imaginary parts of analytic functions which simplifies the task. In addition, if the analytic function does not contain any poles that reside on the jω axis, the real part completely determines the imaginary part for all frequencies and vice versa. The following equations show how the resistance and reactance values are related

$$Z(\omega) = R(\omega) + jX(\omega) \tag{5.2}$$

$$R(\omega) = -\frac{1}{\pi}\int_{-\infty}^{+\infty}\frac{X(\lambda)}{\lambda-\omega}d\lambda + R(\infty) \tag{5.3}$$

$$X(\omega) = \frac{1}{\pi}\int_{-\infty}^{+\infty}\frac{R(\lambda)}{\lambda-\omega}d\lambda \tag{5.4}$$

By assuming the function has no poles on the jω axis, we develop what is known as a *minimum-reactance function*, which means that by determining only the resistance of the impedance function, the reactance is also automatically determined. Therefore, the computation time is reduced by half. It should be noted that the explanation of the RFM that follows is a condensed version of information found in the literature [11]-[12]. For a more detailed derivation, the reader is directed to these sources.

The first step in the RFM is to take the frequency range of the antenna design and discretize it into a series of matching frequencies $0<\omega_1<\omega_2<\omega_3<\cdots<\omega_n$. Knowing the antenna impedance at these points, it is necessary to determine Z_q to maximize the TPG in (5.1)

for the entire frequency range. To take advantage of the impedance relation, the values of the resistance R_q are split into a number of linear segments so that it can be realized by the following summation

$$R_q(\omega) = r_0 + \sum_{k=1}^{N} a_k(\omega) r_k \tag{5.5}$$

where r_0 represents the dc resistance of the system. To make the summation copy the form of the resistance function, the values of $a_k(\omega)$ are determined by a step function

$$a_k = \begin{cases} 1 & \omega_k \geq \omega \\ 0 & \omega_k \leq \omega \end{cases} \tag{5.6}$$

and the r_k's are a series of slopes that represent the resistance curve. By finding the set of slopes that optimize the TPG function, a piecewise linear impedance function is developed for the matching network. Using the impedance relation from (5.2)-(5.4) the reactance can broken up similarly by

$$X_q(\omega) = \sum_{k=1}^{N} a_k(\omega) r_k \tag{5.7}$$

which uses the same values for the r_k's, and the b_k's are found by the integral

$$b_k = \frac{1}{\pi(\omega_k - \omega_{k-1})} \int_{\omega_{k-1}}^{\omega_k} \ln\left|\frac{y+\omega}{y-\omega}\right| dy \tag{5.8}$$

which can be evaluated in closed form by

$$b_k = \begin{cases} C[2\omega_k \ln(2\omega_k) - (2\omega_k - \Delta)\ln(2\omega_k - \Delta) - \Delta \ln \Delta] & \omega = \omega_k \\ C[(2\omega_k - \Delta)\ln(2\omega_k - \Delta) - 2(\omega_k - \Delta)\ln 2(\omega_k - \Delta) - \Delta \ln \Delta] & \omega = \omega_{k-1} \\ C[(\omega_k - \omega)\ln(\omega_k - \omega) - (\omega_{k-1} + \omega)\ln(\omega_{k-1} + \omega) & \textit{otherwise} \\ \quad + (\omega_{k-1} - \omega)\ln|\omega - \omega_{k-1}| - (\omega_k - \omega)\ln|\omega - \omega_t| \end{cases}$$

$$C = \frac{1}{\pi\Delta} \qquad \Delta = \omega_k - \omega_{k-1} \tag{5.9}$$

Once the piecewise linear curve has been determined, the RFM requires that the piecewise linear curve is approximated by a rational function. Using a rational function in the

form of (5.10) leads to an impedance function that can be realized in a two-port cascaded circuit.

$$R_q = \frac{A\omega^2}{1 + B_1\omega^2 + B_2\omega^4 + \cdots + B_n\omega^{2n}} \tag{5.10}$$

From the rational resistance function, the roots of the denominator are found. Retaining only those that reside on the left-half of the plane, a polynomial can be formulated with those roots. This polynomial becomes the denominator of the impedance function.

$$Q(s) = [s + (r_1 + jx_1)][s + (r_1 - jx_1)]\cdots[s + (r_m + jx_m)][s + (r_m - jx_m)] \tag{5.11}$$

We assume that the numerator of the impedance function has the same form as Q(s).

$$Z_q = \frac{a_0 s^n + a_1 s^{n-1} \cdots a_{n-1} s + a_n}{Q(s)} \tag{5.12}$$

This equation can be broken up into even and odd parts of both the numerator and denominator which, in general form, is

$$Z_q = \frac{e_n(s) + o_n(s)}{e_d(s) + o_d(s)} \tag{5.13}$$

Since the rational resistance function is known, equating even and odd parts allows us to solve for the a_n coefficients.

$$R_q = \frac{e_n(s)e_d(s) - o_n(s)o_d(s)}{e_d^2(s) - o_d^2(s)} \tag{5.14}$$

We are left with an impedance function that is a quotient of polynomials that can be realized in circuit form.

$$Z_q = \frac{a(s)}{Q(s)} \tag{5.15}$$

This quotient of polynomials undergoes long division to generate forms resembling (5.20)-(5.21). Each value must be normalized with respect to the operating frequency so the component values must be scaled by an appropriate factor.

5.2 Computer Implementation

Two methods of computer implementation of the impedance matching process were examined. The first followed the method described earlier, while the second represented a modification of this method and has not been fully developed.

5.2.1 Implementation of the real frequency method

For computer implementation, FORTRAN was chosen due to its complex mathematics ability along with the availability of subroutines for optimization [13]-[15]. The Real Frequency Method was easily adapted to the computer, and the algorithm followed the same three phases as described in Section 5.1. In the program, *match.f* , the user is asked to identify the input data file which contains the discretized impedance information of the arbitrary antenna. The data file is organized as a listing of resistance, and reactance for each testing frequency. The user is then asked to enter the frequency units and dc resistance along with the frequency range to be examined. The program presents a list of the input data points allowing the user to select the matching points from the list for the optimization routine. This feature allows variable discretization and the definition of subranges. The user then has the option of weighting the optimization of each matching frequency. This initializes the first optimization routine. For this approach, a subroutine using a Levenberg-Marquardt algorithm optimized the expanded TPG equation given by

$$T(\omega) = \frac{4R_L(\omega)\left[r_o + \sum_{k=1}^{N} a_k(\omega) r_k\right]}{\left[R_L(\omega) + r_o + \sum_{k=1}^{N} a_k(\omega) r_k\right]^2 + \left[X_L(\omega) + \sum_{k=1}^{N} b_k(\omega) r_k\right]^2} \tag{5.16}$$

by solving for the values of the r_k's that minimize the error function.

$$E = \sum_{k=1}^{N} \left[1 - T(\omega_k)\right]^2 \tag{5.17}$$

The second step was to approximate the piecewise linear curve by a rational function. To simplify the calculation of the coefficients, the values were normalized with respect to ω^2 and inverted giving the polynomial

$$R_{qr} = C_0 + C_1\omega^2 + C_2\omega^4 + \cdots + C_n\omega^{2n} \tag{5.18}$$

whose function values and derivatives are easily calculated. Since the resistance function should be positive for all ω, this is tested by the program, and the value of the constant term is kept positive to ensure a finite positive starting point.

After determining the rational function, the program solves for the roots of the denominator, finds the left-hand-plane roots, and multiplies the roots to create the denominator of the impedance function. Knowing the denominator, the coefficients of the numerator are evaluated by using a matrix subroutine to solve the system of equations given by taking the real part (resistance) of the impedance equation and equating the numerators of (5.10) and (5.14). The equations form a diagonally filled matrix in the form

$$\begin{bmatrix} \pm Q_1 & \pm Q_3 & \pm Q_5 & \cdots & 0 & 0 & 0 \\ 0 & \mp Q_2 & \mp Q_4 & \cdots & 0 & 0 & 0 \\ 0 & \pm Q_1 & \pm Q_3 & \cdots & \pm Q_n & 0 & 0 \\ \vdots & \vdots & \vdots & \ddots & \vdots & \vdots & \vdots \\ 0 & 0 & \pm Q_1 & \cdots & \pm Q_{n-2} & \pm Q_n & 0 \\ 0 & 0 & 0 & \cdots & \mp Q_{n-3} & \mp Q_{n-1} & 0 \\ 0 & 0 & 0 & \cdots & \pm Q_{n-4} & \pm Q_{n-2} & \pm Q_n \end{bmatrix} \begin{bmatrix} a_1 \\ a_2 \\ a_3 \\ \vdots \\ a_{n-2} \\ a_{n-1} \\ a_n \end{bmatrix} = \begin{bmatrix} 0 \\ 0 \\ 0 \\ \vdots \\ 0 \\ A \\ 0 \end{bmatrix} \tag{5.19}$$

Now that the values for all coefficients of the impedance function are known, the problem turns to circuit realization. Due to the method of formulation, the numerator will always be of one order less than the denominator which allows for different forms of realization. Given this form, Darlington [16] has shown that any positive-real function (e.g., resistance) can be realized as a cascaded LC circuit terminated with a resistance. Both circuit realizations are developed by performing long division of the impedance function. The first method consists of a fraction expansion about infinity which would have the general form

$$Z_q(s) = \cfrac{1}{C_1 + \cfrac{1}{L_1 + \cfrac{1}{C_2 + \cfrac{1}{L_2} + \cfrac{1}{R_1}}}} \tag{5.20}$$

The second method removes a term and then continues with an expansion about infinity

$$Z_q(s) = \cfrac{1}{\cfrac{1}{L_1} + C_1 + \cfrac{1}{L_2 + \cfrac{1}{C_2 + \cfrac{1}{R_1}}}} \tag{5.21}$$

Of course, the size of these long divisions and, consequently, the number of components necessary to realize the circuit, varies with the order of the rational function used to approximate the piecewise linear curve. The orientation of the circuitry components goes from the antenna on the left side of the equation to the generator at the right. Skeptics will point out that the resistance found closest to the generator does not comply with the desire for a loss-less network. This, however, can be realized by placing a transformer between the generator and the matching network. In order to realize a circuit, the values contained in the cascaded fraction must be normalized to the testing frequency unit.

Two versions of the program were produced. The first code utilized IMSL [14] routines available on the University of Illinois CONVEX main frame. The desire to generate a portable program with operational control of the subroutine parameters led to a second version which was written using subroutines from Numerical Recipes [15]. Table 5.2 lists the subroutines and uses for both codes. The optimization routine in each case used a Levenberg-Marquardt algorithm for minimization. This method is based on using a steep descent method with points far from a minimum, and switches to an inverse-Hessian method as the guess approaches the minimum. Although the methods were the same, the Numerical Recipes code required the formulation of the derivatives to be supplied which seemed to decrease computational time. In addition, IMSL optimization was limited by user-defined maximum

number of iterations, which if exceeded caused program termination. The Numerical Recipes subroutine allowed a more subtle alternative for cases that did not seem to converge.

Table 5.1 Listing of computer subroutines used in the impedance matching program.

Purpose	IMSL	Numerical Recipes
Optimization	**DUNLSF**	**MRQMIN**
Root Finding	**ZPLRC**	**ZROOTS**
Matrix Solution	**DLSARG**	**LUDCMP**

5.2.2 Implementation of the modified real frequency method

Although work continues on this form of implementation, results look promising at this time. The modification of the RFM removes the requirement for two optimization loops by optimizing for the impedance function directly. By generating an array of coefficients, the impedance function can be written as

$$Z(s) = \frac{A_{\deg} s^{\deg-1} + \cdots + A_2 s + A_1}{A_{2\deg} s^{\deg} + \cdots + A_{\deg+2} s + A_{\deg+1}} \tag{5.22}$$

where deg indicates the user-defined resolution of the impedance function. These coefficients are chosen to minimize the error function in (5.17). By utilizing this modification, the separate calculation of linear and rational functions is avoided and the subroutines for root finding and matrix solving are not needed. Therefore, this method is advantageous not only because one optimization loop yields a realizable circuit, but also because both the resistance and reactance are optimized simultaneously. In the Real Frequency Method, the rational function optimization dealt with the resistance function alone. The reactance was determined from the solution of the impedance function coefficients. The reactance value was therefore removed from the optimization process. Differences in the linear and rational reactance functions can be significant, which lead to problems in the realization of an impedance matching network.

Section 5.3.2 shows a case where the failure to optimize the reactance value yields poor TPG results.

Three problems were encountered when implementing the modified system. First, the derivatives for the TPG function in terms of the impedance function coefficients were extremely complex. Therefore, a finite difference method was implemented to solve for each of the derivatives. Next, the problem of optimizing to a local minima was noticed. To solve this difficulty, the initial guess for the minimization routine was randomly chosen for multiple trials. The best result of these trials became the final optimization. The final difficulty dealt with the impedance function coefficients. The optimization routine was modified to force each coefficient of the function in terms of s (where s -> $j\omega$) to a positive value. This insured that the output function could be realized by a matching network. Some preliminary results are included in the following results summary.

5.3 Computer Results

The computer results for the impedance matching program have been mixed. For some antenna geometries, the TPG has increased appreciably across the entire frequency range tested. At the same time, some antenna geometries were ill-conditioned for the subroutines, which forced the research towards developing improved techniques to implement the Real Frequency Method for arbitrary antennas.

5.3.1 Resistively loaded linear monopole

The first test case was originally tested by Ramahi [12] which served as a TPG comparison. The test antenna was a 12 m monopole with a 7.5 cm radius and had a 240 Ω series resistance placed 6.9 m from the base. The size sets the resonance at 625 MHz, but the impedance match was desired for 2-9 MHz. Therefore, the antenna measured approximately 0.32 λ at the lowest testing frequency. Impedance values for the antenna shown in Figure 5.3 were loaded into the program. After the first optimization loop, the computer produced the

piecewise linear resistance curve and its corresponding reactance which are plotted in Figure 5.4. The TPG was improved across the frequency band for the antenna as seen in Figure 5.5 which shows the unmatched TPG (TPG with a 50 Ω cable connected directly to the monopole) vs. the matched TPG with the piecewise linear matching impedance. The computer then executed the second optimization loop to determine a rational approximation of the piecewise linear resistance curve. A comparison of the piecewise linear curves and the rational impedance curves is shown in Figure 5.6. It is important to note that in the RFM, the piecewise linear reactance is derived directly from the resistance using Cauchy-Riemann theorems. During the second loop, only the resistance curve is approximated. The rational imaginary part comes solely from the derivation of the impedance function using the equations in Section 5.1. Note that there is a significant difference between the rational and linear reactances. This fact can greatly hamper matching for some antenna systems, which is why the modified method was implemented.

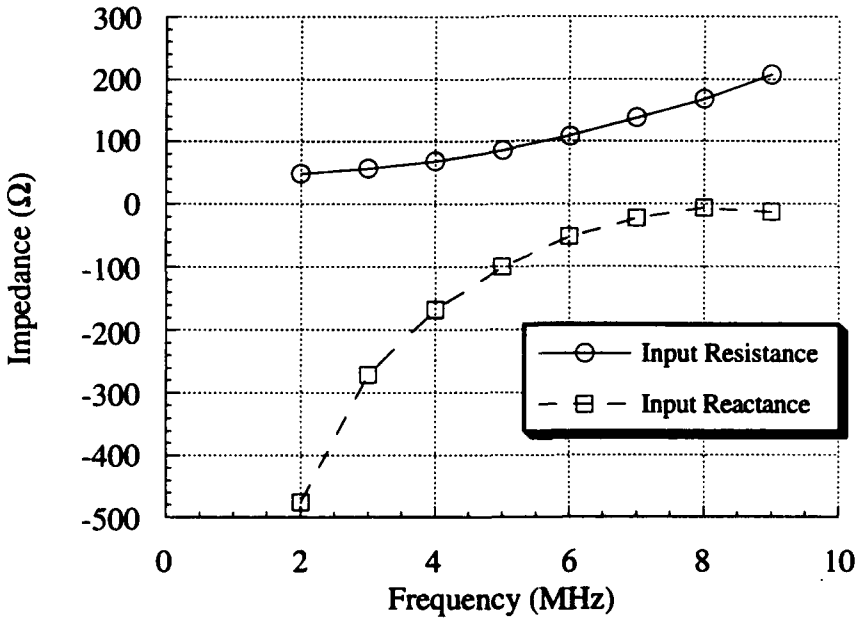

Figure 5.2 Test antenna input impedance [12].

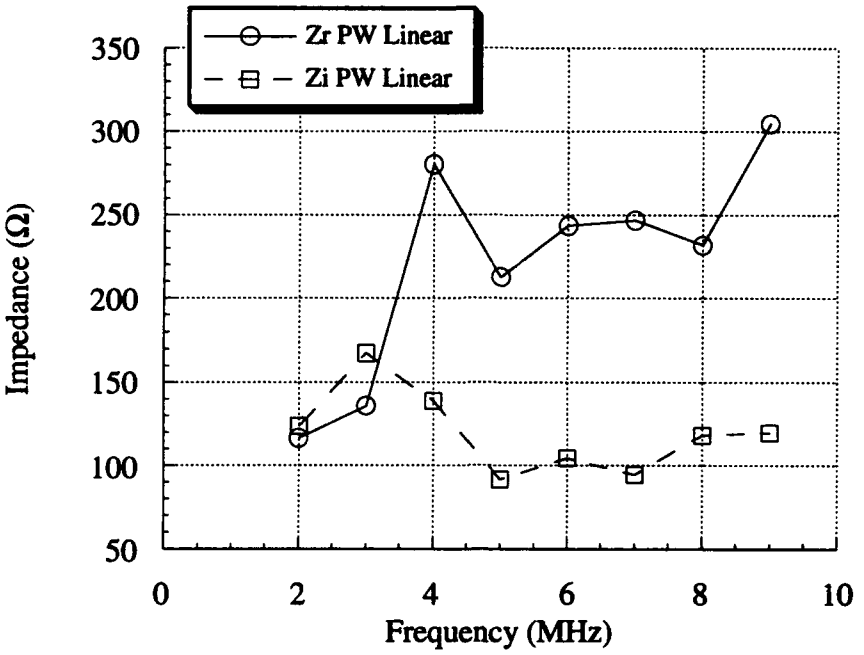

Figure 5.4 Piecewise linear impedance curves for maximum TPG.

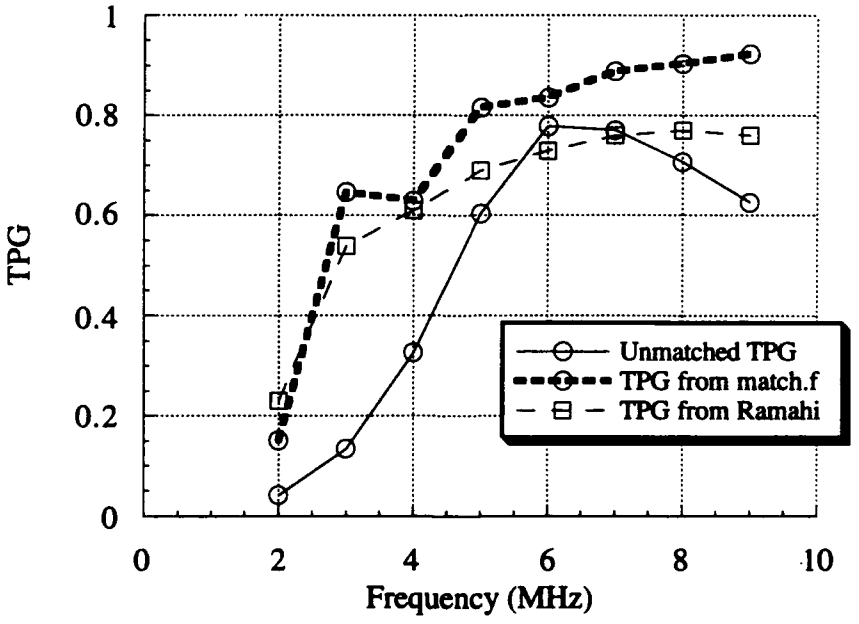

Figure 5.5 TPG comparison after piecewise linear optimization.

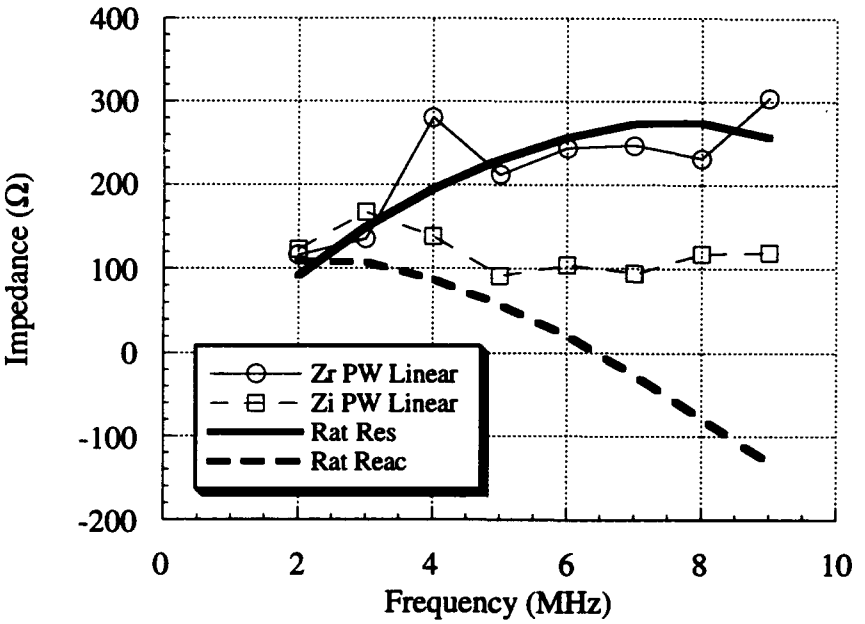

Figure 5.6 Comparison of piecewise linear impedance function and the rational function approximation.

Once the rational resistance has been found and, therefore, the rational impedance function is known, the realized TPG can be plotted to compare with the piecewise linear and unmatched values. Figure 5.7 contains the TPG values for each case and includes the results from the previous analysis for comparison. Notice that for higher frequencies, the results from *match.f* are superior, and low-frequency values match those from the literature [12]. In an effort to further improve the performance, the low frequency TPGs were weighted to increase those values. Since the matching problem represents a compromise, if the TPGs for one part of the frequency band increase, they will do so at the expense of some other part of the band. Figure 5.8 shows the change in TPG after the weighting was implemented. The program appears to work quite well, and depending on the shape of TPG curve desired, weighting can be applied but not without degradation in other places.

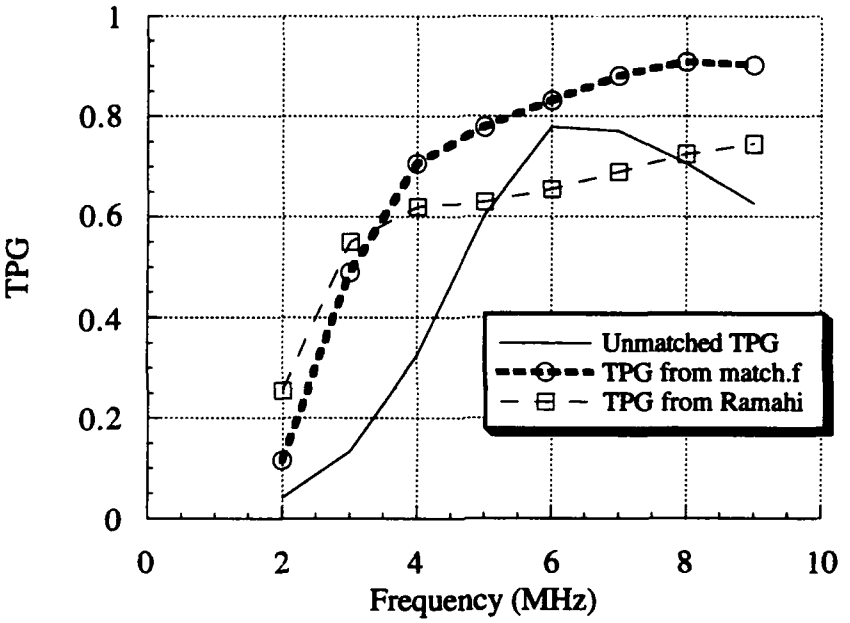

Figure 5.7 Realized TPG comparison for *match.f* and Ramahi [12].

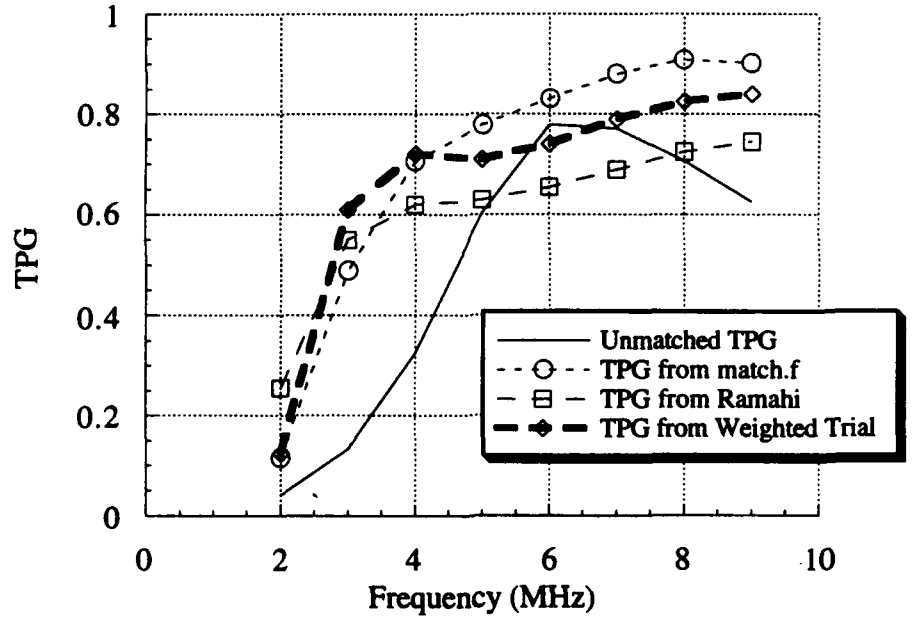

Figure 5.8 Realized TPG comparison including weighted case.

The final step in the analysis is to develop the impedance matching network. Taking the impedance function for the unweighted case, two forms of long division are performed to yield the components for the matching network. Both of the matching network circuits appear in Figure 5.9. Remember that the resistance at the generator end will be approximated by using a transformer to limit device losses. Time for construction of these circuits for experimentation was not available, but Ramahi [12] fabricated similar circuits for experimental performance analysis.

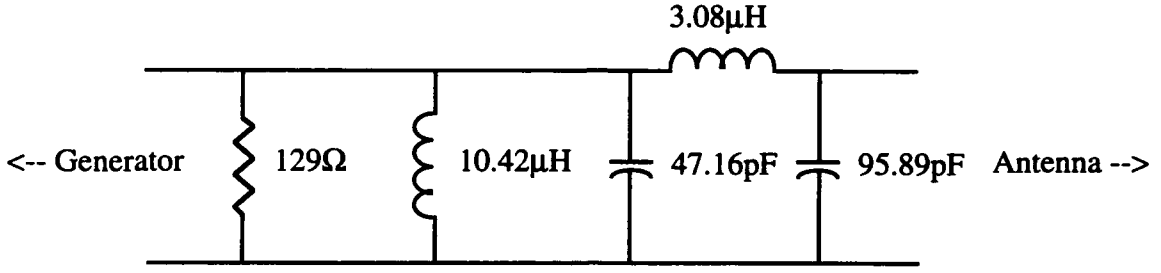

Figure 5.9(a) Matching network circuit realization using expansion about infinity.

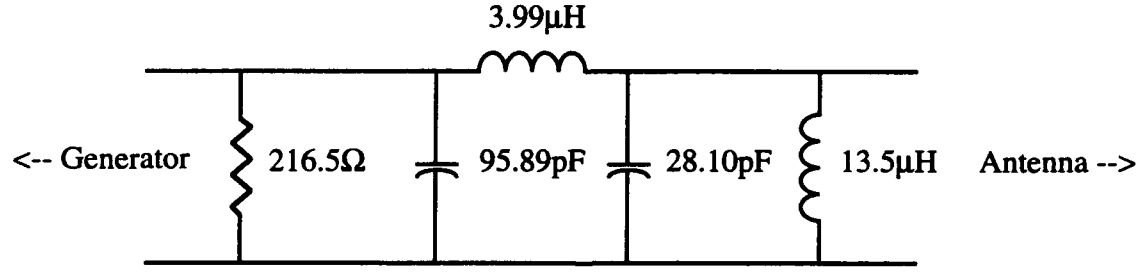

Figure 5.9(b) Matching network circuit realization using expansion about infinity after removing one term.

5.3.2 Folded gamma

The folded gamma presented much more of a problem to match than the linear monopole. Even though the design itself produced decent TPG characteristics as seen in Figure 5.10, it was hoped that the results could be improved with a matching network. After the first optimization, it appeared that this was possible as seen in Figure 5.10. The problem presented itself in the second optimization. Since the piecewise linear curve showed a sharp

increase at the highest frequency, the program would fit the curve with a function that contained poles along the jω axis that caused a discontinuity in the resistance curve and negative resistances for higher frequencies. To keep the resistances positive, points were added to the piecewise linear model to guide the curve back to zero. The "dying slope" also made a difference in the matching results. Some antenna models required a steep dying slope to offer maximum TPG while others needed a more gradual slope. To remedy this problem, a subroutine was written to iterate through various slopes, increasing the number of points as the slope decreased. Although this slightly degraded the minimization between the matching frequency piecewise and rational resistance points, it insured a realizable circuit.

Continuing with the analysis, Figure 5.11 shows the shape of the piecewise linear function and its corresponding rational approximation. The slope at the end is the product of following the dying slope generated in the program. When the rational function was realized in circuit form, the TPG appeared as depicted in Figure 5.12. Notice that the TPG drops off for high frequencies. Since the resistance function seems to be approximated well by the rational function, the drop must be caused by the difference between the piecewise linear and rational approximations of the reactance. Preliminary results show that the modified program can improve this TPG curve since both resistance and reactance are optimized simultaneously. Figure 5.13 shows a comparison between the realized TPGs for both optimization methods. Notice that the curve generated by the modified RFM improves the matching characteristics of the folded gamma geometry for all test frequencies. Figure 5.14 contains the values for the impedance of the matching network.

5.3.3 Tank circuit loaded linear monopole

This final analysis was still in the experimental stages during the writing of this thesis. The model consists of a linear monopole with tank circuit and resistive loading for multiple band current choking. Although a final design was not chosen, Figure 5.13 contains a listing of unmatched, piecewise linear, and multiple rational function TPG results. It should be noted

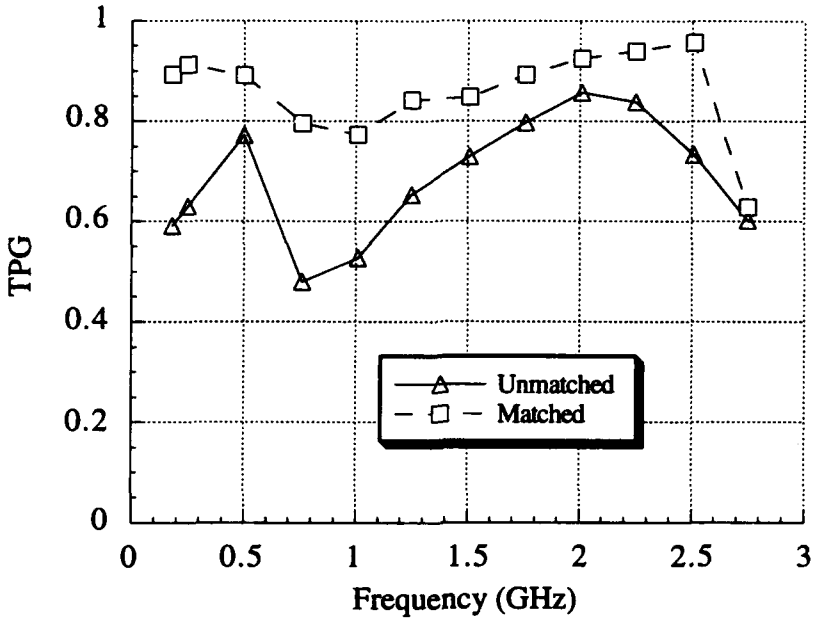

Figure 5.10 TPG comparison: unmatched vs. piecewise linear match.

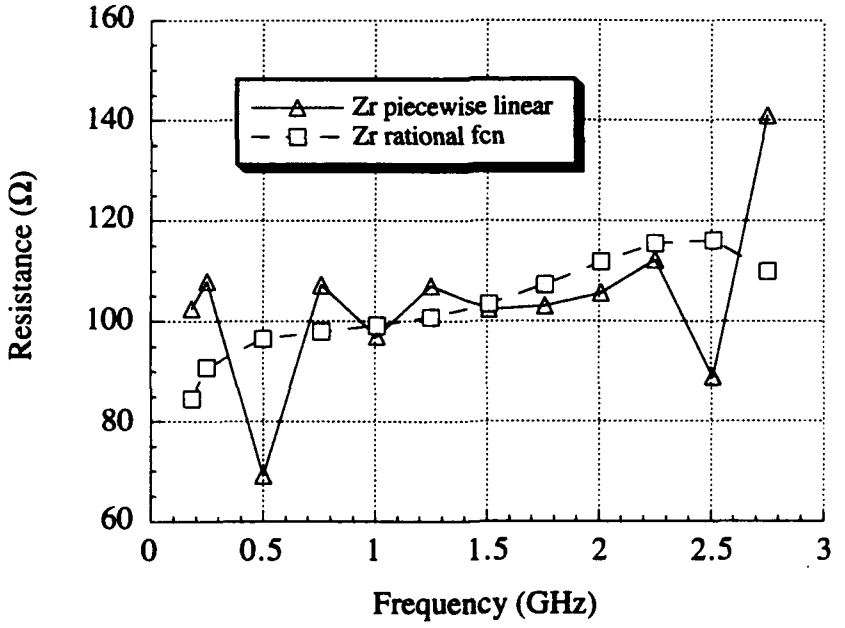

Figure 5.11 Matching network resistance functions, piecewise linear and rational.

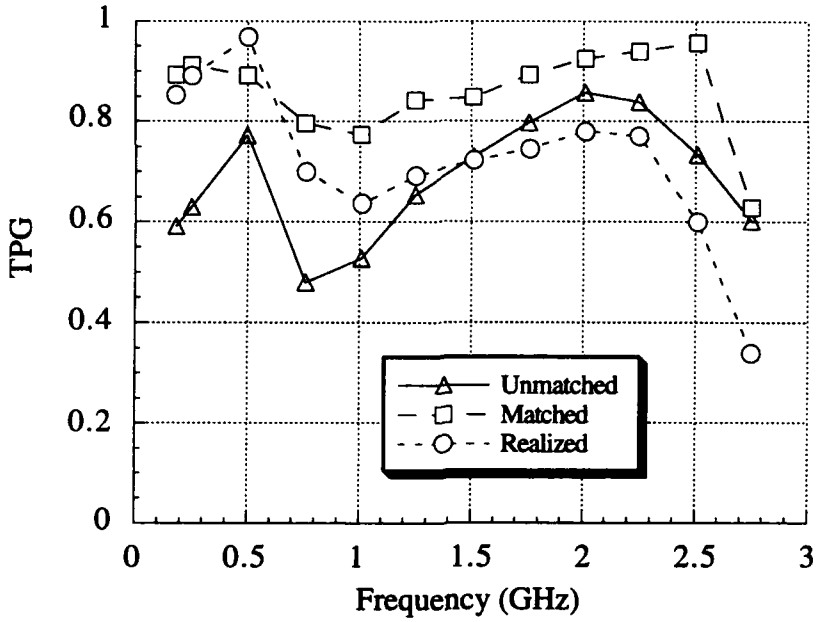

Figure 5.12 Final TPG comparison for each stage of RFM optimization.

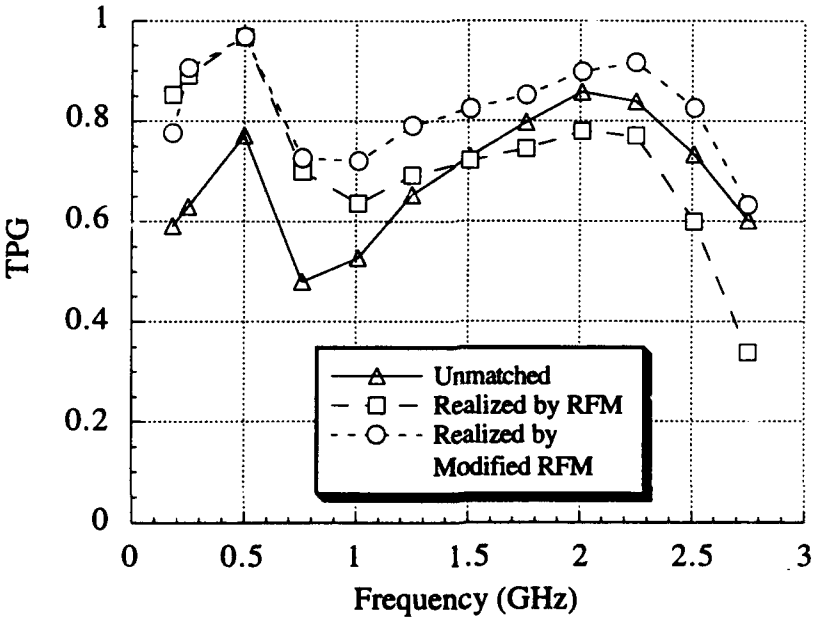

Figure 5.13 Realized TPGs for both optimization methods.

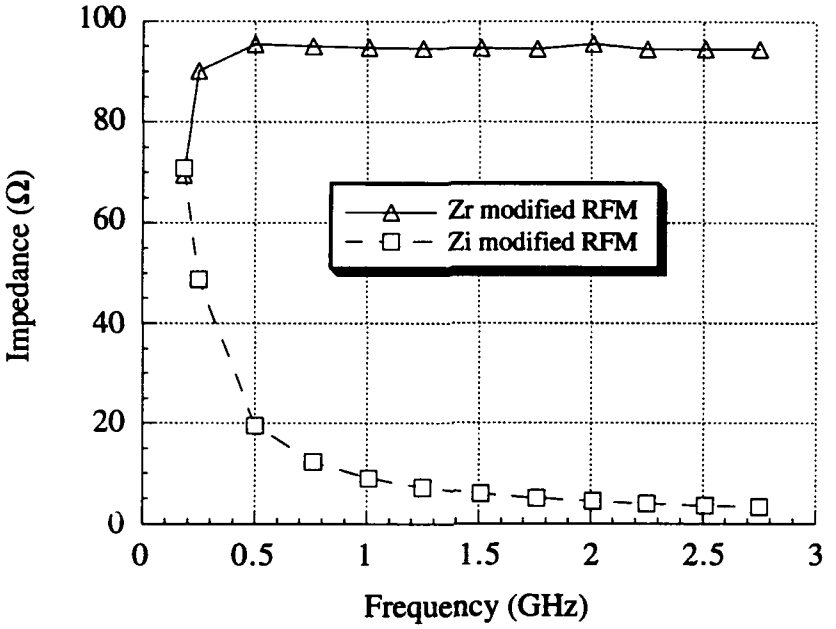

Figure 5.14 Matching network impedance from modified RFM.

that with the RFM, since the rational function optimization attempts to match the piecewise linear curve, it is unlikely that the performance will exceed that of the first optimization loop. In the case of this antenna, there exists a band that appears ill-conditioned for matching. Some compromises must be made since every antenna cannot be matched across every frequency range. This brings about the possibility of multiple matching networks, or multiple feeds to correct this TPG drop. In Figure 5.15, multiple trials were performed during the rational function approximation. The program not only allows frequency weighting of the TPG values for optimization, but the user can also choose the degree of the rational function approximation. It is interesting to note that a third order approximation seems to have the optimum matching capability for this particular antenna design. This antenna has yet to be optimized using the modified RFM.

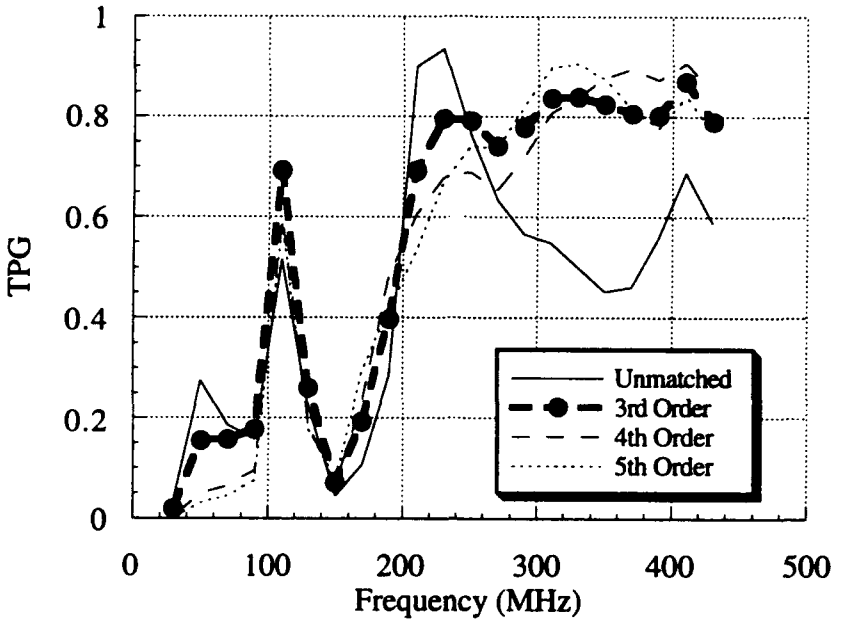

Figure 5.15 TPG Comparison for a tank circuit loaded linear monopole.

5.4 Future Modifications

The code has demonstrated limitations that could be corrected. Work is currently being performed complete the implementation of the modified method. The modification not only reduces computation time by combining the optimization loops and removing the need for root finding and matrix equation solving, it also allows for the simultaneous optimization of both the resistance and reactance of the matching function. Once completed, this method should offer significant improvements to the design of impedance matching networks, which can optimize the performance of arbitrary antenna structures.

6. CONCLUSIONS

To develop a design for a low-profile broadband monopole vehicle antenna, numerous methods of geometry alteration and loading were analyzed. Although neither of these concepts alone could significantly improve the characteristics of the antenna to acceptable limits, a combination of the two appeared optimum. The desire for easily matched impedance performance was balanced by the need of a low elevation directed omnidirectional pattern. The Numerical Electromagnetic Code was used for computer analysis of the models that were then fabricated for experimentation in the laboratory.

NEC remains a powerful tool for the analysis of wire structure antennas. Although deviations between numerical and experimental data were noted early in the research, the addition of parasitic capacitance and careful modeling of lumped components corrected the problem. These modifications made NEC a reliable method to quickly examine changes in geometry and loading. Because the software package was limited in its ability to model sleeve structures, analysis of these devices was performed in the laboratory.

Application to military vehicles necessitated the use of simple, durable antenna geometries. Design modifications were implemented on a linear monopole to fulfill the low-profile requirement while increasing broadband performance. It was determined that increasing the length of the conductor as well as antenna volume improves characteristics. However, these structures can become too complicated and space intensive which makes them impractical for a ground-based communication system. During the analysis, compromises were made between the impedance characteristics and the omnidirectional performance of structures. Variations of the linear monopole such as the "T" and "Kite" geometries did not yield significant improvements. The gamma geometry looked promising and its variants, the "Y" and "X" monopoles, were studied in depth. The final geometric change included the use of crossed arrays for multiband operation.

Beyond the geometric modifications, loading techniques were also considered. The variations in reactive components at high frequencies precluded their use in the designs.

Lumped resistive loading, however, produced significant improvement throughout the frequency band. Series-loaded and tip-loaded monopoles were tested to optimize impedance and pattern characteristics. Grounded sleeves were studied due to the limitations of computer modeling, and produced low-frequency impedance improvement. Termination loading was also examined for multiantenna systems in order to minimize coupling between radiating and nonradiating elements.

The research yielded a folded gamma design with promising results for the frequency range from 180 MHz to 3 GHz. The used of resistive tip loading and geometric concepts developed earlier produced an antenna with excellent impedance characteristics and a reasonably omnidirectional radiation pattern throughout the frequency range. The analysis of arrays yielded a design that operates well in three frequency bands with omni-directional characteristics.

Chapter 5 of this thesis deals with the implementation of the Real Frequency Method for arbitrary antenna structures. The results were mixed since some antennas showed vast TPG improvement while some seemed ill-conditioned for the method. The lack of a rational reactance optimization in the RFM led to a modification of the method that combined the two optimization loops to solve for the impedance function coefficients directly. The RFM also had to be altered to insure that the resistance function remained positive for all frequencies. Despite these failings, the program worked for all three antennas tested for the research. There is no doubt that the RFM is a powerful method for developing matching network circuitry, with no mathematical assumptions made about the load or network transfer functions. The preliminary results for the modified RFM are promising. By optimizing the impedance function in one step using finite differences for derivative evaluation, computational time decreases and a better match is produced since both resistance and reactance are optimized simultaneously. The implementation of these circuits enables the antennas to achieve maximum broadband performance.

REFERENCES

[1] H. A. Wheeler , "Fundamental limitations of small antennas," *Proc. IRE*, vol. 35, pp. 1479-1484, December 1947.

[2] G.J. Burke and A.J. Poggio, "Numerical Electromagnetic Code (NEC)-Method of Moments, Part III: User's Guide," Lawrence Livermore National Laboratory, January 1981.

[3] R. W. P. King, *The Theory of Linear Antennas*, Harvard University Press, Cambridge, MA, 1956.

[4] L. Little, "Broadbanding techniques for some wire structure antennas," M.S. thesis, University of Illinois at Urbana-Champaign, Urbana, Illinois, 1993.

[5] E. Anderson, "Coplanar waveguide dual-feed patch elements and a log-periodic array thereof," M.S. thesis, University of Illinois at Urbana-Champaign, Urbana, Illinois, 1992.

[6] "HP8510B Network Analyzer: System Manual," Hewlett-Packard Co., April 1988.

[7] D. W. Smith, "The automated pattern range," Electromagnetics Laboratory Report No. 91-1, May 1991.

[8] G. H. Brown and O. M. Woodward, Jr., "Experimentally determined radiation characteristics of conical and triangular antennas," *RCA Review*, vol. 13, no. 4, December 1952.

[9] E. E. Altshuler, "The traveling-wave linear antenna," *IRE Trans. Antennas Propagat.*, vol. AP-9, pp. 324-329, July 1961.

[10] W. L. Stutzman and G. A. Thiele, *Antenna Theory and Design*, John Wiley & Sons, Inc., pp. 108-167, 1981.

[11] H. J. Carlin, "A new approach to the gain-bandwidth problem," *IEEE Trans. Circuit Syst.*, vol. 24, pp. 170-175, April 1977.

[12] O. Ramahi, "Synthesisizing matching networks for high-frequency antennas using the real frequency method," M.S. thesis, University of Illinois at Urbana-Champaign, Urbana, Illinois, 1986.

[13] M. J. Merchant, *Fortran 77: Language and Style*, Wadsworth Publishing Co., 1981.

[14] *User's Manual, IMSL Math/Library: FORTRAN Subroutines for Mathematical Applications*, IMSL, Inc., 1989.

[15] W. H. Press, B. P. Flannery, S. A. Teukolsky, and W. T. Vetterling, *Numerical Recipes: The Art of Scientific Computing*, Cambridge University Press, 1989.

[16] S. Darlington, "A survey of network realization techniques," *IRE Trans.*, vol. CT-2, pp. 291-297, December 1955.